Turbulent mixing in the near bottom layer on the central Namibian shelf

Master's Thesis

at the
Leibniz Institute for Baltic Sea Research (IOW)
Warnemünde

submitted by

Tom Lange

Institute of Physics
University of Rostock

Rostock, 18 February 2015

Supervisor and first Reviewer: Dr. Volker Mohrholz, IOW
Second Reviewer: Dr. Martin Schmidt, IOW

Abstract

The Benguela upwelling system stretches along the coast of south-western Africa and is one of four major eastern boundary upwelling systems of the World Ocean. The region is characterized by intense primary production, which causes fishing to be a substantial industrial activity. As a result, there is a lot of interest and need to improve the understanding of the basic physical and biological processes that determine the variability of this ecosystem.

Furthermore, long-shore alternating bands of high and low concentrations of organic matter are observable in the surfical sediments on the central Namibian shelf. Generally, many dynamic processes are known to drive sedimentation and re-suspension in the benthic boundary layer, but there is still a lack of understanding concerning the role of each process towards the pattern of spatial variability of organic matter.

Thus, the purpose of this Master's thesis is to improve the understanding of the short-term variability on the central Namibian shelf. Secondly, it aims to answer the question: Which turbulent processes control the turbulent mixing in the near bottom layer on the inner shelf off Walvis Bay, Namibia.

In order to approach these objectives, a wide range of data was accessible. The crucial element of the data was gathered during a cruise on the central Namibian shelf in January 2013. After many steps of analysis and calculations, the obtained results were plotted and investigated for several processes.

After studying all possible processes, one can conclude that the turbulent mixing in the near bottom layer on the inner shelf off Walvis Bay is mainly determined by shear-induced turbulence. However, the corresponding bed shear stresses are too small to cause re-suspension of sediments. The variability of shear-induced turbulence is controlled by a superposition of different processes, whereby low-frequency continental shelf waves and coastal trapped waves with periods of several days probably generate the largest currents in the near bottom layer. Moreover, waves like swell or non-linear internal waves are easily observable on the central Namibian shelf, but their contribution on turbulent mixing in the bottom boundary layer on the inner shelf seem to be negligible.

The comparison of the magnitudes of the turbulent kinetic energy dissipation rate at the shelf break with the inner shelf position reveals several significant differences. At the shelf break, strong dynamical processes seem to generate enhanced turbulent mixing in the oceanic boundary layers as well as in the interior of the water column. It can be seen that the general distribution of spots of intense turbulence coincide with the regions of low concentrations of organic matter across the central Namibian shelf.

If all findings are taken together, one can conclude that the inner shelf off Walvis Bay supports the sedimentation of light organic matter due to two reasons: firstly, the bottom shear stresses are too small to generate significant re-suspension. Secondly, the flat inner shelf region appears to be a 'shadow zone' for energetic dynamical processes that have a significant impact for steeper topography, such as at the self break or in the surf zone.

Contents

Contents v

List of Figures vii

1 Introduction 1
- 1.1 Motivation . . . 1
- 1.2 Outline . . . 2
- 1.3 Benguela upwelling system . . . 2
- 1.4 Central Namibian shelf . . . 5

2 Theory 11
- 2.1 Turbulence . . . 11
  - 2.1.1 Measurements of oceanic turbulence . . . 12
  - 2.1.2 Turbulence in the near bottom layer . . . 13
  - 2.1.3 Shear turbulence and law of the wall . . . 13
  - 2.1.4 Turbulence in the stratified ocean . . . 14
- 2.2 Important mixing processes . . . 15
  - 2.2.1 Swell . . . 16
  - 2.2.2 Internal waves . . . 17
  - 2.2.3 Continental shelf waves and coastal trapped waves . . . 20

3 Material and methods 23
- 3.1 Hydrographic observations . . . 23
  - 3.1.1 RV Mirabilis cruise MOM1301 . . . 23
  - 3.1.2 Moorings . . . 25
  - 3.1.3 Remotely sensed data and weather observations . . . 26
- 3.2 Methods of analysis . . . 27

4 Results and analysis 29
- 4.1 Environmental conditions on the central Namibian shelf . . . 29
  - 4.1.1 Meteorological conditions . . . 29
  - 4.1.2 Sea surface temperature . . . 29
  - 4.1.3 Transects along the 23°S line off Walvis Bay . . . 32
  - 4.1.4 Temporal variability of hydrographic conditions . . . 32
  - 4.1.5 Variability of near bottom temperatures . . . 35
- 4.2 Characteristics of turbulence in the near bottom layer . . . 36
- 4.3 Identification of significant dynamic processes . . . 37
- 4.4 Analysis of the swell variability . . . 39
- 4.5 Study of non-linear internal waves . . . 41
- 4.6 Turbulence caused by bed shear stress . . . 44
- 4.7 Characteristics of turbulence across the central Namibian shelf . . . 47

5 Discussion and conclusion 49

Bibliography 53

List of Figures

1.1 Map of Southwestern Africa . . . 3
1.2 Spatial distribution of mud belts . . . 7

2.1 Logarithmic velocity profile . . . 14
2.2 Generation of an internal tide . . . 18
2.3 Reflection of internal wave beams . . . 19

3.1 Detailed map of measurement area . . . 25
3.2 Sketch of deployed moorings . . . 26

4.1 Weather conditions in Swakopmund in January 2013 . . . 30
4.2 Distribution of sea surface temperature (SST) . . . 31
4.3 Hydrographic conditions along the 23°S line . . . 33
4.4 Time series of CTD measurements . . . 34
4.5 Time series of MSS measurements . . . 35
4.6 Near bottom temperatures . . . 36
4.7 Time series of TKE dissipation rate . . . 37
4.8 Power spectrum from pressure time series . . . 37
4.9 Power spectrum from time series of the horizontal velocities . . . 38
4.10 Observation of swell in January 2013 . . . 40
4.11 Steps and results of NLIW investigation . . . 41
4.12 Surface expression of NLIW off central Namibia . . . 42
4.13 Investigation of NLIW by the vertical velocity . . . 44
4.14 Time series of the Thorpe length scale L_T . . . 45
4.15 Time series of the gradient Richardson number . . . 46
4.16 Comparison of processes . . . 46
4.17 TKE dissipation rate along the Walvis Bay transect . . . 47
4.18 Comparison of TKE dissipation rates . . . 48

Chapter 1

Introduction

1.1 Motivation

The continental shelf seas of the World Ocean are very variable and complex areas as well as regions of intense physical and biological activity (Liu et al., 2000). Especially the available sunlight in the shallow waters and the often nutrient enriched surface layer provide excellent conditions for biological production. As a result, ocean margins are an important source of food; fishing is a substantial industrial activity for the neighbouring countries, and thus contributes significantly towards the economic welfare of the region (Carr and Kearns, 2003; Lamb, 2014).

Due to that, there is a need to elucidate the basic physical and biological processes that determine the shape and variability of the ecosystem. While the hydrographical conditions of surface water can be studied in detail with satellite data, the observation of the subsurface layers is far more complicated. However, the physical processes in the whole water column are of crucial importance. They govern the reversible motion and the irreversible small-scale mixing of water and its constituents, and accordingly they are subjected to the shelf-water features and many fluxes (Huthnance, 1995).

In particular, the various dynamical characteristics of the bottom boundary layer give rise to a lot of interest. Turbulent mixing of mass, momentum and heat take place in that region, resulting in particles, chemicals and organisms being exchanged between the seabed and overlying water column (Grant and Madsen, 1986). For these reasons, the study of the turbulence in the ocean is a key element in the investigation of the ocean's processes and their energetics.

The knowledge and understanding regarding turbulent processes below the ocean's surface layer, and specifically in the near bottom layer, are still incomplete. But nevertheless, they are critical for the appreciation processes in that area, such as re-suspension and sediment distribution (Inthorn et al., 2006a).

Furthermore, turbulent processes act on various time scales. Thus, studies involving elaborate and expensive measuring methods with a high temporal resolution are needed to conduct a comprehensive analysis. However, there have been relatively few studies in the coastal ocean that attempted to study the full range of potential turbulent processes on the continental shelf and their impact on the near bottom layer.

The central Namibian shelf is part of the Benguela upwelling system, which is one of four major eastern upwelling regions, where cold, nutrient-rich deep waters are injected into the surface mixed layer, enabling intense primary production (Inthorn et al., 2006a). A unique feature of this region arises from an interesting spatial variability of organic matter concentration in the bottom sediments. Alongshore belts of enhanced organic matter concentrations parallel to the isobaths were discovered many years ago on the central Namibian shelf (e.g. Bremner, 1983), but still there is only limited understanding about the origin of this complex pattern. Past studies suggest evidence that turbulent processes may contribute

to that observed belt structure of organic matter (Monteiro et al., 2005), but they were not able to prove their hypothesis with observations from required high temporal resolution data. Nevertheless, it is prerequisite to identify and understand the major mixing processes to realistically model the circulation and biological processes in shelf seas and to effectively predict their response to climate change.

In order to approach this challenge, the foundation of this study is based on a large data set with many high temporal measurements in the whole water column. The used observations were performed on the inner shelf off Walvis Bay, Namibia, during austral summer in 2013 and were analyzed with respect to their temporal variability.

Thus, the aim of this work is to at least improve the understanding of the short-term variability of the turbulent processes on the central Namibian shelf and to answer the question: Which turbulent processes dominate the mixing in the near bottom layer on the inner shelf?

The treatment of the chosen objectives should contribute to the overall understanding of how the different dynamics control the mixing in the near bottom layer and thereby provide clarification about the exceptional structure of the organic matter concentration across the central Namibian shelf.

1.2 Outline

The purpose of this thesis is not only to present and discuss the findings from the gathered data, but also to introduce features of the Benguela upwelling system, the central Namibian shelf and the relevant turbulent processes. To accomplish the written goals, the framework of the thesis is arranged as follows. The first introductory part will shortly review the Benguela upwelling system and demonstrate the characteristics of the central Namibian shelf, including the unique belt structure of enhanced organic matter concentrations, based on past studies. The definition, description and influence of turbulence and the different turbulent processes on the central Namibian shelf are the focus areas of the second chapter. The following part is intended to describe the used data and the measuring procedure. Furthermore, it outlines the approach and methods, which have been used during the study. The forth chapter presents and highlights the results of the analysis. Finally, a discussion and conclusion of the most important findings complete this thesis.

1.3 Benguela upwelling system

In a brief review of a complex and versatile ecosystem such as the Benguela upwelling system it is ambitious, if not impossible to cite all relevant literature without making this paragraph unreadable and the thesis along with it. Accordingly the list of references is by no means exhaustive, but it should be adequate to serve as an introduction into the system and to lead into the remainder of the literature available on the Benguela ecosystem and into more specialized disciplinary literature.

The large scale hydrology of the South East Atlantic and comprehensive descriptions of the Benguela upwelling system have been reviewed by a number of authors (e.g. Hart and Currie, 1960; Shannon, 1985; Nelson and Hutchings, 1983; Shannon and Nelson, 1996; Shillington, 1998; Stramma and England, 1999; Carr and Kearns, 2003; Hutchings et al., 2006; Shillington et al., 2006).

The Benguela upwelling system stretches along the coast from the southern tip of Africa northwards to the Angola-Benguela frontal zone (ABFZ) located at about 15°-16°S and encompasses the full extent of Namibia's marine environment (Bakun and Nelson, 1991). A schematic representation by Boyer et al. (2000) is shown in Figure 1.1 and illustrates the main oceanographic features, bathymetry and surface circulations of the Benguela upwelling system. The so-called Benguela Current is a broad northward flow off south-western Africa and is part of the subtropical gyre of the South Atlantic.

The Benguela is one of four major eastern boundary current upwelling systems of the world ocean and is dominated by wind-driven coastal upwelling, similar to the California, Peru and north-west Africa cur-

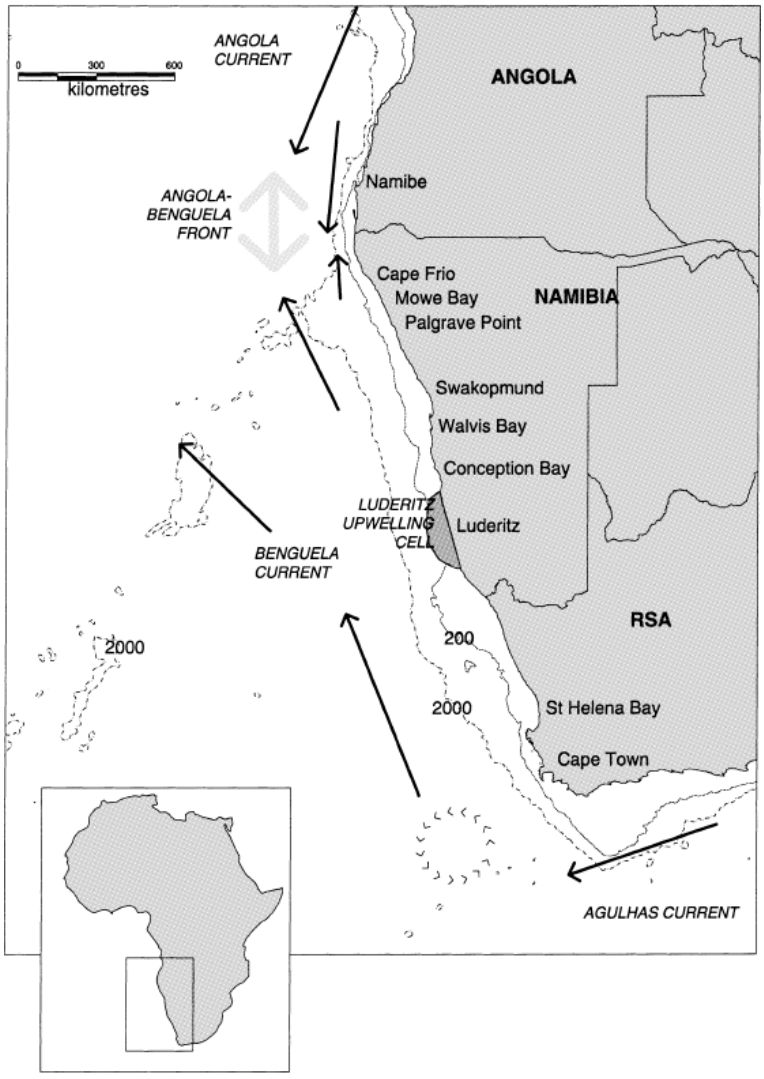

Figure 1.1: Map of Southwestern Africa, with schematic illustration of the main oceanographic features, bathymetry and surface circulation. Taken from Boyer et al. (2000).

rent systems. What makes the Benguela upwelling system unique in the global context is its open warm-water boundary at the southern and northern ends, with the retroflection area of the Indian Ocean's Agulhas Current and the equatorial eastern Atlantic, respectively (Shannon and Nelson, 1996; Shillington, 1998).

The area of the Benguela is exposed to a persistent equatorward wind associated with the St. Helena high pressure system centred over the South Atlantic Ocean. This upwelling favourable alongshore wind has its possessive maximum at about 25°S and decreases towards the northern and southern boundaries of the Benguela system (Bakun and Nelson, 1991). The alongshore northward wind stress leads to an Ekman transport in the surface boundary layer which is then directed offshore. The existence of the coastal boundary evokes a horizontal divergence in the surface layer, emerging in upwelling near the coast. Subsequently, cold nutrient-rich subsurface water reaches into the euphotic zone inducing the observed high biological productivity (e.g. Shannon and Nelson, 1996), which is among the highest on our planet (Carr and Kearns, 2003). The euphotic zone is the surface layer in the ocean which is sufficiently illuminated to permit photosynthesis by phytoplankton (Hutchings et al., 2006). The coastal upwelling is confined to a coast band with a width of the baroclinic Rossby radius (Fennel, 1999), which is approximately 200 km along the Namibian coast.

The surface Ekman offshore transport must be compensated by an onshore flow at greater depth, due to the conservation of mass. As the flow passes over the sloping bottom of the coastal ocean, the adjust-

ment of potential vorticity drives wave propagation and subtidal fluctuations in velocity, which propagate poleward along the eastern boundary of southwest Africa. Thus, most of the observed variability in the alongshore flow over the shelf can be interpreted as so-called coastal trapped waves (CTW) with periods in the range of 3 to 10 days. Nevertheless, if these low-frequency fluctuations are removed from the signal, the prevailing mean flow near the bottom on the shelf is in poleward direction at a mean speed of about 5 km per day (Nelson, 1989; Brink, 1991). Besides the wind-driven Ekman transport and the coastal trapped waves, additional processes also play a significant role for the coastal dynamics. The Benguela upwelling system displays a high degree of variability over a broad spectrum of time and spatial scales, which will be considered in the following chapters.

In the extreme south, the winds are highly seasonal due to a shift in the atmospheric pressure systems and an increased influence of westerly winds during austral summer. Easterly moving cyclones south of Africa on time scales of about 3 to 10 days lead to pulsed upwelling events (Shannon and O'Toole, 2003). In the central and northern Benguela, the seasonal variation is weaker, with the most pronounced upwelling during late winter and spring (Shannon and Nelson, 1996). The upwelling also appears to be less pulsed off Namibia, since the influence of the eastward-moving cyclones is diminished with decreasing latitude (Shannon, 1985). Furthermore, the diurnal heating and cooling of the land leads to a diurnal character of the wind (land-sea breeze effect), especially in regions where periods of relaxation of winds are common (Hart and Currie, 1960; Shannon and O'Toole, 2003).

Moreover, the equatorward wind stress varies not only in the alongshore direction, it also increases seaward resulting in a band of cyclonic wind stress curl along the coast, forcing increased coastal upwelling (Fennel, 1999).

Aspects like the width of the continental shelf, the presence of capes and the strength of the local equatorward wind stress determine the resultant wind-induced upwelling (Bailey and Chapman, 1991). As a result, there are seven particularly active upwelling centres present in the Benguela, of which the Lüderitz cell (25°-26°S) is by far the most intense regime. The cell forms a natural internal divide within the Benguela, with the domains to the north and south of it behaving in rather different ways (Shannon and O'Toole, 2003; Hutchings et al., 2006).

The southwest coastline of Africa stretches in an almost north-north-east direction from the Cape of Good Hope, South Africa to about 18°S and is incised by only a few embayments and major capes, of which most exist in the southern part (Shillington, 1998). The entire length of the coast is characterized by a confined coastal belt of flat land, constantly ascending to a high interior plateau at about 130 km to 160 km inland. North of 30°S, this coastal belt is a desertlike region that extends to about 14°S and is known as the Namib Desert (Hart and Currie, 1960). Owing to the extremely arid nature of the climate at the south-western coast of Africa, freshwater input to the coastal ocean is not significant except in sporadic times of summer flooding in the interior of the country (Nelson and Hutchings, 1983).

The continental shelf off southern Africa, defined approximately by the 200 m contour line, strongly varies in the Benguela region. A relatively wide shelf can be found off the Orange River mouth (140 km), at Agulhas Bank in the extreme south (230 km), and off Walvis Bay (110 km). North of 20°S, the shelf narrows and off southern Angola is almost non-existent, the slope falling straightaway from the coast into the depth of the Angola Basin (Hart and Currie, 1960). Other narrow shelves exist south of Lüderitz (40 km) and off the Cape Peninsula (40 km) (Figure 1.1).

The deep ocean basin offshore of the Benguela, the so-called Cape Basin, is bounded in the north by the Walvis Ridge which runs from the coast at about 18°S in a south westerly direction, to link up with the central Atlantic Ridge in the South Atlantic (Nelson, 1989). The Walvis Ridge forms a very effective barrier to northward movement of the Antarctic bottom water below 3000 m (Hart and Currie, 1960; Nelson and Hutchings, 1983).

In contrast to other major upwelling systems, the Benguela contains large hypoxic and anoxic shelf areas beneath the surface layer, which have strong impact on the recruitment strategies of many species populating these regions (Woodhead et al., 1998). Particularly off southwest Africa, there is a very rapid

decrease with depth in the inshore waters, so that even in normal conditions in this region the content of dissolved oxygen is less than 1 ml/l in the near bottom layer on the continental shelf (Hart and Currie, 1960). This widespread oxygen minimum zone (OMZ) expands from the inner shelf across the upper continental margin (Inthorn et al., 2006b). Thereby, the variability of dissolved oxygen in the water masses is controlled by several biological processes in the coastal ocean, the movement and composition of different water masses and of course the interchange of surface waters with the atmosphere.

1.4 Central Namibian shelf

The preliminary paragraph intends to introduce into the basic features of the entire Benguela upwelling system. The following section shall now limit the area of focus to the characteristics of the central Namibian shelf.

The central Namibian shelf is a favourable spawning area and habitat for pelagic and demersal fish (Bakun, 1993; Hutchings et al., 2006). As already mentioned, several oxygen-depleted or anoxic bottom-water conditions are perennial characteristics over the central Namibian shelf region, specifically between 19°S and 24°S. Much of the shelf shallower than 200 m is covered by a thin layer of oxygen-poor water with an oxygen content of less than 2 ml/l, and locally as little as 0.1 ml/l (Summerhayes, 1983; Nelson and Hutchings, 1983). The variability of the low-oxygen water (LOW) off central Namibia is determined by a complex interaction between remotely forced shelf boundary conditions, seasonal thermocline variability and biogeochemical carbon fluxes (Monteiro and van der Plas, 2006).

Between austral summer and autumn, extremely low concentrations of dissolved oxygen develop over the central Namibian shelf. This oxygen minimum is mainly a consequence of remineralisation of the sedimenting primary production (Bailey and Chapman, 1991), which peaks during spring and summer. Central Namibia is downstream of the major upwelling cell off Lüderitz, which is responsible for substantial organic input into the northern Benguela system. In other words, the sedimenting phytoplankton production contribute to the un-oxidised organic matter on the seabed, resulting in depleted oxygen conditions near the bottom.

Several studies (e.g. Monteiro et al., 2006; van der Plas et al., 2007; Bartholomae and van der Plas, 2007; Mohrholz et al., 2008) emphasise the role of the non-linear interaction between local-scale and remote-scale forcing, which controls the variability of LOW in the northern Benguela system. It appears that beside the local biogeochemical processes, the variability in the advection of two different South Atlantic Central Water (SACW) masses onto the shelf leads to an interannual variability in the dissolved oxygen concentration of the Namibian shelf. Those water masses are namely the hypoxic SACW of tropical origin and the more aerated Eastern SACW (ESACW). The hypoxic and nutrient-rich SACW is advected by the poleward undercurrent into the northern Benguela during austral summer, while oxygen-rich ESACW extends northwards during the upwelling season in austral winter (Mohrholz et al., 2008). Thus, a permanent convergence zone of the Central Water masses exists off central Namibia between Lüderitz and northern Namibia.

Although the driving processes and scales of impact of hypoxia and anoxia in the northern Benguela are not clearly understood yet, one can resume that the low-oxygen conditions appear to result from a combination of local remineralisation of organic matter, as well as advection of remotely sourced oxygen-poor water (e.g. Bartholomae and van der Plas, 2007).

It is also worth mentioning that the presence of hypoxic conditions on the Benguela continental shelf can impact on the local biota greatly and is responsible for periodic mortalities of demersal fish and bottom species. These events are common in the Walvis Bay region and sometimes accompanied by eruptions of hydrogen sulphide gas (Hart and Currie, 1960). High rates of sedimenting organic matter joined by weak vertical mixing and horizontal advective fluxes in the near bottom layer lead to perennial sediment anoxia, resulting in sulphide and methane gas bubble fluxes into the overlaying water column

(Emeis et al., 2004; Monteiro et al., 2005). Outbreaks of toxic sulphide gases are a seasonally (austral summer) repeating feature in the near-coastal shelf environment offshore Namibia and thus, they have a significant economic and societal relevance because of their effects on biota (Emeis et al., 2004).

Moreover, benthic organisms are not only limited in their distribution by water depth and hydrodynamic processes, but also the oxygen content of the bottom water plays a significant role (Summerhayes, 1983).

The wind off northern and central Namibia shows relatively little seasonal variation, there are nevertheless slight maxima in the upwelling favourable wind during April to May and October (Shannon, 1985). Northerly wind and calm weather conditions at Walvis Bay can lead to a stagnation of the circulation and therefore intensify the depletion of oxygen in the near bottom water layer (Hart and Currie, 1960).

The main shelf break in the central Namibian region is at 360 m to 400 m water depth at about 160 km offshore. Close to Walvis Bay, the shelf is broad, and a second, minor shelf break is observable at about 140 m water depth some 100 km offshore.

Distribution of organic matter

As previously indicated, the central Namibian shelf depicts a unique spatial variability of organic matter concentrations on the seabed. The sediment composition, structure and bathymetry of the central Namibian shelf have been described by Bremner (1983),Summerhayes (1983) and Inthorn et al. (2006b).

As well as the bathymetry, the composition and physical characteristics of the surficial sediments can be helpful to gain a broad understanding of the dynamics of a shelf system.

The western continental margin of southern Africa is dominated by biogenic sedimentation resulting from the high productivity of the upwelled waters in the Benguela system. Thus, the sediments are mainly composed of calcium carbonate ($CaCO_3$), organic matter and opal (Bremner, 1983; Inthorn et al., 2006b).

Bremner (1983) collected 792 surficial sediment samples between 10 m and 1500 m depth on the Namibian shelf, and Inthorn et al. (2006b) gathered sediment samples at additional 95 stations to obtain the geochemical information from the surface sediments on continental margin offshore south-western Africa. Their investigations revealed the following results: Sediments rich in opal and organic carbon are deposited in a narrow belt on the inner shelf off central Namibia. Their distribution and facies are controlled by water depth, the current and wave energy at the sea floor, biological productivity (both pelagic and benthic), terrigenous input and diagenesis (Bremner, 1983). However, input by terrestrial organic matter to the southwest African shelf is low due to the absence of perennial rivers at the arid coast, except for the Orange River in the south (Summerhayes, 1983; Shannon and Nelson, 1996). The biogeochemical processes at the sediment-water interface are determined by very high accumulation rates of organic material which result in high oxygen consumption rates and high sulphate reduction rates at the sea floor (Emeis et al., 2004, and references therein).

Concentrations of organic carbon (OC) in surface sediments reveal a heterogeneous distribution across the central to northern Namibian shelf. The spatial variability is characterised by an alongshore banding structure. Thereby, two particulate organic matter depleted bands separate three relatively organic-rich sediment bands of 500 to 800 km length (Figure 1.2; Bremner, 1983; Inthorn et al., 2006b).

A more comprehensive examination on the mud belts (Figure 1.2) expose an inner shelf mud belt with highest concentrations of organic carbon (7-12 %) at depth of 50-140 m, a mid-shelf belt at depths of 200-300 m (4-8 %) and an outer shelf belt at depths of 500-1400 m (4-9 %).

The most inshore coast-parallel belt of diatomaceous mud is confined to, and extents almost continuously, on the inner part of the Walvis shelf between 19° to 26°S. The continuity of the mud belt is broken at one place (north of 21°S) where, according to Bremner (1983), wave activity at the crest of a 50 m deep shoal prevents the settling of diatomaceous debris onto the sea floor. The concentration is greatest

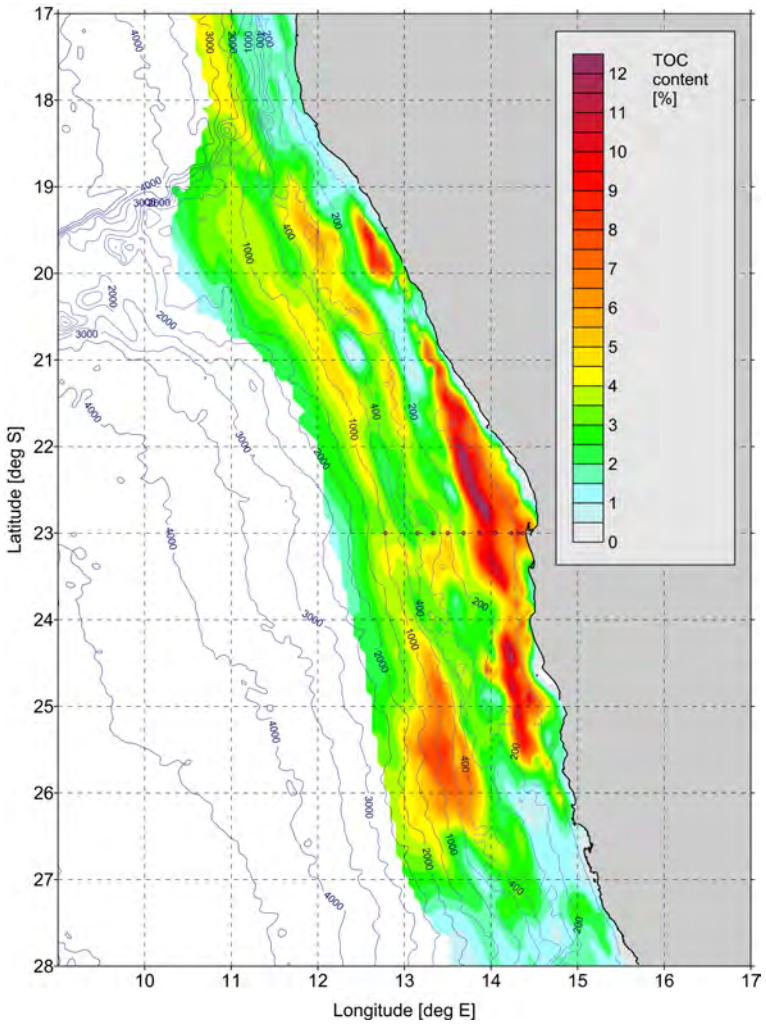

Figure 1.2: Spatial distribution of total organic carbon content (TOC) in surface sediments off central Namibia. Large-scale bands with high and low concentration of particulate organic matter are observable along the Namibian Shelf. Taken and modified from Inthorn et al. (2006b).

40 km offshore off Walvis Bay (23°S) with typical values of 12 %. The other two belts of organic-rich sediment extend on the mid shelf and upper slope, the former between 19°-23°S, and the latter between 19°-27°S (Figure 1.2). The mid shelf deposit stretches along the offshore side of the mid shelf break at around 250 m depth, and the upper-slope deposit coincides approximately with the 1000 m isobaths. The age of the diatomaceous mud belts is estimated to be around 3,000 (Inthorn et al., 2006b) to 5,000 years (Bremner, 1983).

The explanation of the observed spatial distribution is not straitforward and very challenging because a combination of various physical and biological processes contributes to the distribution of organic matter across the continental shelf. In recent decades, several authors (e.g. Bremner, 1983; Summerhayes, 1983; Bailey and Chapman, 1991; Monteiro et al., 2005; Inthorn et al., 2006b,a) have tried to improve the understanding, but the knowledge is still incomplete.

Undoubtedly, the rate of sedimentation is significant in preserving the organic matter that reaches the bottom. The factor generally responsible for productivity in the region is the prevailing equatorward wind. Its intensity is strongest in the vicinity of Lüderitz where upwelling is most active and perennial. Here, nutrients brought to the surface are then transported northwards by the Benguela Current in the broad coastal embayment at Walvis Bay, where the productivity has its maximum (Summerhayes, 1983). The diatom-dominated high productivity forces the sedimentation of organic matter where turbulence does not prevent organic particles from settling. Organic matter is mainly transported to the bottom in

fecal pellets (Bremner, 1983) and thus, the oxygenation of the water column has little effect on sinking particles (Summerhayes, 1983). That means, the settled organic matter will be preserved, with some loss by diagenesis, if it is buried at a reasonable rate, regardless of the oxygen content of the bottom waters. Owing to the high primary production, shallow water depth, and bottom-water oxygen depletion, the burial of organic matter is highest above the inner shelf and leads to the characteristic organic-rich, anoxic mud of the inner shelf (Inthorn et al., 2006b,a).

Another important control of preservation of organic-rich surface sediments is the amount of oxygen in bottom waters. Demaison and Moore (1980) defined waters having an oxygen content less than 0.5 ml/l as anoxic, considering that it is the threshold at which bioturbation by benthic organisms becomes substantially depressed, which is certainly the case on the inner shelf off Walvis Bay (Bailey and Chapman, 1991).

However, a spatial variability in the occurrence of oxygen-deficient water arises in the Benguela upwelling system from the fact that wind-induced coastal upwelling systems are characterized by isolated centres of upwelling rather than a ribbon of continuous upwelling within the Benguela system (Shannon, 1985; Shannon and Nelson, 1996). For instance, south of 26°S, towards the Lüderitz upwelling centre, the concentration of dissolved oxygen, overlying the sediments, increases rapidly while phytoplankton abundance in the surface water layer and abundance of organic carbon in surface sediments simultaneously decrease (Figure 1.2; Bailey and Chapman, 1991).

In contrast, there is little temporal variability in the incidence of oxygen-deficient bottom waters overlying the shelf of Walvis Bay. Because of the lack of seasonality in upwelling along the coast (Shannon, 1985), the sediment oxygen demand and carbon flux is high throughout the year above the highly organic diatomaceous mud belt (Bailey and Chapman, 1991). In other words, the associated turbulence due to perennial upwelling near Lüderitz does not support high phytoplankton productivity (Hart and Currie, 1960). In the Walvis Bay region, the presence of reduced wind stress, a decrease in wind-induced upwelling and enhanced solar heating results in horizontal and closely spaced isopycnals, which stabilize the water column (Bailey and Chapman, 1991), causing strong biological productivity and sedimentation of organic matter, subsequently.

Several actions could influence the formation and persistence of the two deeper deposition centres. The lower concentration of organic matter could result from the longer settling times of the organic particles. Remineralisation of the organic particles during settling trough the water column is more intense due to the higher water depth so that comparatively few particles reach the seafloor (Bremner, 1983). Furthermore, Inthorn et al. (2006b) suggested strong remobilisation and lateral export of organic matter from shelf areas toward the slope and the deep sea during periods of rapid sea level change as a major factor leading to the formation of the two deeper deposition centres. Additionally, the deeper long-shore belts of organic-rich sediments are outside the upwelling front from where most of the new production is exported. For this reason, the study of Inthorn et al. (2006b) highlights the importance of lateral transport in the Benguela upwelling system of modern carbon production and burial.

The inshore mud belt seems to be sustained by the combined forcing of phytoplankton-new-production-fluxes owing to coastal upwelling, the seasonal stratification of the water column, low content of oxygen in the bottom waters (Summerhayes, 1983) and a persistently low bed shear-stress in this area (Monteiro et al., 2005).

Many physical processes can influence the distribution of particulate organic matter on continental margins. Among others these include: tides, waves, wind-driven coastal currents, coastal upwelling and sediment re-suspension (Liu et al., 2000). The bed stresses generated by gravity waves may account for the low concentration of organic matter closest to the coast line in less than 50 m depth (Rogers and Bremner, 1991; Monteiro et al., 2005).

Suspiciously low content of organic carbon on the outer shelf and along the shelf edge support the hypothesis of locally prevailing erosion (Monteiro et al., 2005; Inthorn et al., 2006b). Due to that, Monteiro et al. (2005) investigated the role of internal tides in controlling the sedimentation and re-suspension

of particulate organic matter on the central Namibian shelf and their impact on the distribution of the long-shore alternating bands of high and low concentrations of organic matter. They hypothesise that the continuous energy dissipation in the vicinity of the shelf break leads to bed shear-stresses which drive re-suspension in the benthic boundary layer inshore of the shelf break zones and thus determine the banding structure of particulate organic matter. This is supported by the fact that highest values of suspended particulate matter in the bottom boundary layer were found close to the shelf break site, which confirm their assumption that the shelf break regions are non-depositional areas (Inthorn et al., 2006a). It has been further indicated that the regions with low concentrations of organic matter coincide with areas where the topographic slope angle is critical for internal tide reflection (Inthorn et al., 2006a). Moreover, the study has shown that the critical shear-stress distribution across the central Namibian shelf corresponds with the predicted net accumulation and net erosional areas of particulate organic matter. More specifically, the sites that are characterized by lowest average benthic boundary layer current velocities and bed shear-stresses are those where the highest concentrations of organic matter appear (Monteiro et al., 2005). Taking their findings together, they suggested that the barotropic-baroclinic tidal coupling controls the vertical particle flux dynamics, whereas Ekman and inertial flows are thought to control the horizontal advection scales which lead to the observed spatial variability of organic matter (Figure 1.2). However, due to their very limited data and an only hourly sampling rate of the sensors, they were neither able to prove the hypothesis nor could they analyse the influence of high-temporal turbulent processes on the re-suspension of sediments.

Chapter 2

Theory

This chapter is intended to provide an insight into background information about the hydrographical and turbulent processes, which were analysed in this thesis. As well as explaining basic principles, the chapter presents a variation of commonly used formulas.

2.1 Turbulence

The following remarks are intended serve as an introduction to turbulence and especially to turbulent characteristics in the near bottom layer. The setup and content are mainly taken from the textbooks of Thorpe (2007) and Cushman-Roisin and Beckers (2011).

Turbulence is a stochastic flow phenomenon, which is observable in diverse fluids and gases. There is no simple and explicit definition of the term *turbulence*. Nevertheless, turbulent motions can be understood as a population of many eddies, each of different size and strength, embedded within one another and forever changing, giving a random character to the flow. As a result of this complexity, a generally valid theory is lacking, and turbulence is still one of the major unsolved problems of classical physics (Burchard and Umlauf, 2013). However, on the basis of observations and different types of modelling approaches, it is possible to present a few properties that are generally accepted for turbulent flows in the ocean and other naturally occurring fluids: 1) Turbulent flows depict a random character in time and space. Due to that, statistical quantities, rather than a deterministic description of individual turbulent fluctuations, are used to specify turbulence. 2) The turbulent motions generate sharp gradients and increased contact surfaces within the fluid, resulting in greatly increased mixing and transport rates. As a consequence, turbulence is not only the dominant physical process in the transfer of momentum and heat, but also in dispersing solutes and small particles in the ocean (Thorpe, 2007). 3) Turbulent flows are associated with eddies that comprise a huge range of spatial wave lengths, ranging from the largest scales set through the bounding geometry towards the smallest scales, where these eddies are dissipated due to the impact of molecular viscosity. 4) Thus, turbulence transports kinetic energy from the largest scales, where energy is introduced into the system, down to the smallest scales, where the kinetic energy is dissipated into heat by viscous friction.

The primary cause of turbulence manifests in the instability of flows, which tends to occur when inertial forces become large compared to other forces in the momentum balance. This situation can be expressed by the *Reynolds number*,

$$Re = \frac{\mathcal{U}\mathcal{L}}{\nu}, \tag{2.1}$$

which compares the magnitude of inertial to frictional forces and is always very large in turbulent flows. In the above relation, $\mathcal{U}$ stands for mean flow velocity, $\mathcal{L}$ for the relevant length scale and ν is the viscosity of the water. The non-dimensional Reynolds number alone describes the transition from laminar to turbulent flows, whereby the transition typically occurs for $Re = \mathcal{O}(10^3)$ (Burchard and Umlauf, 2013).

Since the natural state of the ocean is one of turbulent motion, knowledge of turbulence and its effects is crucial to understanding the characteristics of the ocean and to construct numerical models. These models intend to predict how the ocean will adjust, since the forcing by the atmosphere is modified by changes in the world's climate (Thorpe, 2007). A key step on the way to increased knowledge of turbulence is to measure, observe and analyse turbulence.

2.1.1 Measurements of oceanic turbulence

As mentioned before, turbulence is a form of motion containing kinetic energy that is dissipated and transferred into heat much faster than in a laminar flow. This behaviour represents an irreversible loss of kinetic energy from the ocean. The measure of this dissipation is commonly expressed as the rate of dissipation of turbulent kinetic energy (TKE) per unit mass, commonly denoted by ε with units of W/kg (Thorpe, 2007). The rate of loss of the kinetic energy of the turbulent motion per unit mass through viscosity to heat can be expressed in general as

$$\varepsilon = (\nu/2)\langle s_{ij} s_{ij} \rangle, \tag{2.2}$$

where the velocity is written as (u_1, u_2, u_3) in three orthogonal directions $x = x_1$, $y = x_2$ and $z = x_3$, and ν is the kinematic viscosity. The tensor s_{ij} is given by $s_{ij} = (\partial u_i/\partial x_j + \partial u_j/\partial x_i)$, and products are taken over repeated indices i, j = 1 to 3. The complexity of the expression for ε hints that its accurate measurement is generally extremely difficult (Thorpe, 2007).

However, if we assume *isotropic* turbulence, which means that the properties of turbulent motion are the same in all directions, then Equation (2.2) reduces to a much easier form,

$$\varepsilon = (15/2)\nu\langle(\partial u/\partial z)^2\rangle, \tag{2.3}$$

where the average value of any spatial derivative in a direction normal to its direction may be taken. Thus, the assumption of isotropic turbulence substantially simplifies the measurement requirements, because only one component of the shear needs to be determined in order to estimate the magnitude of the TKE dissipation rate.

In the ocean, values of ε range over many orders of magnitude, starting at about 10^{-10} W/kg in the abyssal ocean to about 10^{-1} W/kg in the most active turbulent regions, such as the surf zone (Thorpe, 2007). The length scale of the turbulent motions at which viscous dissipation becomes important, is known as the *Kolmogorov length scale*

$$l_K = (\nu^3/\varepsilon)^{1/4}. \tag{2.4}$$

For a typical oceanic viscosity of $10^{-10}\,\mathrm{m}^2/\mathrm{s}$, a range of l_K from about 6×10^{-5} m in very turbulent regions to 0.01 m in the abyssal ocean is obtained, if the exemplary oceanic values of ε from above are taken.

At a fixed point of measurement, turbulent eddies are advected at a mean speed U and cause fluctuation in the measured characteristic of turbulence (e.g. velocity fluctuations). Small eddies pass in relatively short times, and thus cause fluctuations of higher frequency than those caused by larger eddies. The time taken by eddies of size l to pass a fixed point is $T = l/U$, and the corresponding measured frequency is $\sigma = 2\pi/T$, which is related to the eddy wavenumber, $k = 2\pi/l$, by $\sigma = kU$. If it is assumed that the eddies do not change significantly while they are passing the measurement point, then it possible to translate temporal measurements in terms of frequency into spatial measurements of wavenumbers. This hypothesis is known as the *Taylor hypothesis* (Thorpe, 2007). If this is true, the measured frequency spectra derived from time series measurements can be converted into wave number spectra.

As already mentioned, one outstanding character of turbulence is the cascading of energy from larger to smaller scales. It is accepted that kinetic energy is introduced into the ocean at relatively large scales, and then is successively passed by interaction between eddies or their instabilities through a spectrum of smaller scales, where inertial forces, rather than viscosity forces, are dominant. In the end, the small

eddies of a size comparable to l_K, 'feel' the viscosity and thus transfer their kinetic energy into heat. This behaviour is also known as the *turbulence cascade*.

Kolmogorov (1941) showed that for very large Reynolds numbers ($Re > 107$) and homogeneous and isotropic turbulence, the *spectral kinetic energy density* (kinetic energy per unit mass per unit wavenumber bandwidth) is given by

$$\Phi(k) = q\,\varepsilon^{2/3}k^{-5/3}, \tag{2.5}$$

within a subrange of wave numbers, where inertial forces dominate over viscous. This range lies between the wave numbers of the large energy-containing eddies in the turbulent field and the Kolmogorov dissipation scale, $2\pi/l_K$. The non-dimensional constant q is empirically found to be approximately equal to 0.5 (Thorpe, 2007).

Simultaneous measurements in three dimensions are often impracticable, so that fluctuations of the velocity in the ocean cannot be determined. Therefore, the variations of velocity are mostly measured in a single direction by lowering a probe attached to a recording instrument. The probe incorporates a piezoelectric crystal, which provides electrical signals proportional to the changes in one component of the lateral force. This force is caused by the relative lateral water speed, produced by the turbulent eddies in the water through which the probe is traversing. The probe is calibrated to convert the rate of change of the force into the shear of the velocity of the flow.

Generally, the size of the probe is too large to resolve fluctuations down to l_K and consequently, it is not possible to directly apply Equation (2.3) to estimate ε. Therefore, spectral estimates of the measured spatial gradients are fitted to a known universal *Nasmyth spectrum* (Nasmyth, 1970). This fitted and interpolated spectrum is then used to obtain estimates of ε by using relations like Equation (2.5).

2.1.2 Turbulence in the near bottom layer

This thesis aims to analyse the variability of turbulence in the bottom boundary layer (BBL). The bottom boundary layer is the region adjacent to the sea floor, where the flow experiences the direct effects of bottom friction, which includes energy dissipation, vertical mixing and extraction of horizontal momentum. Before describing some of the features of the near bottom layer, it is important to note that, whilst boundaries may lead to processes that produce turbulence, the physical presence of the boundaries also modifies the turbulence in their vicinity. Viscous forces near an almost static seabed tend to reduce the components of velocity parallel to the boundary (Thorpe, 2007).

In comparison to the overlying water column, the oceanic BBL is typically characterized by temperature and salinity profiles that are well mixed, by sheared currents parallel to the seafloor, by Ekman veering of horizontal currents and by suspended matter.

2.1.3 Shear turbulence and law of the wall

The term *shear* represents the spatial gradient of the velocity of a current in a direction normal to the direction in which it flows (Thorpe, 2007). A shear flow is illustrated in Figure 2.1, showing that the vertical shear du/dz is non-zero in the vicinity of the sea floor, where u is the horizontal current and z is the vertical distance from the boundary. This vertical shear results in an increase of the distance between particles, which are separated by distances z normal to the flow direction. This means that water particles, initially close together, become detached by turbulence. Thus, the action of turbulence is consequently one of dispersion of material particles by stirring whilst homogenising fluid properties by diffusion. Together these processes lead to mixing which is irreversible.

In the ocean there is a variety of processes that modify the velocity profile of the free-stream flow, like tidal oscillation, the earth's rotation and the vertical density gradients as well as combinations between them. However, in the direct vicinity of the bed, the dynamics of the flow are controlled by the effect of molecular viscosity. This so-called *bed layer* is usually only a few centimetres thick. Above this bed

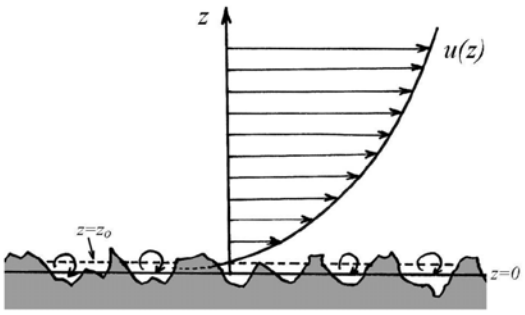

Figure 2.1: Logarithmic velocity profile in the vicinity of a rough bottom. Taken from Cushman-Roisin and Beckers (2011).

layer, the flow mainly depends on the bed shear stress and less on the geometry of the bed (Soulsby, 1983). Therefore, in the case of a steady mean flow and turbulence, energy conservation and a negligible buoyancy flux, the turbulent dissipation ε in a shear flow can be expressed by

$$\varepsilon = (\tau/\rho_b)\, du/dz, \tag{2.6}$$

where $u(z)$ is the mean flow parallel to the sea floor. It is then convenient to define a *friction velocity* u_* with reference to the bed shear stress, according to the relation $\tau_b = \rho\, u_*^2$. Assuming that the motion is independent of kinematic viscosity, the mean horizontal velocity shear, du/dz, solely depends on u_* and on the distance z above the seabed (Thorpe, 2007). Due to dimensional reasons the vertical velocity shear reduces to

$$du/dz = u_*/(\kappa z), \tag{2.7}$$

where κ is the *von Kármán constant* and empirically found to be approximately 0.41 (Cushman-Roisin and Beckers, 2011). The integration of Equation (2.7) leads to the well-known *law of the wall*, describing the variation of the horizontal velocity with distance from the boundary,

$$u(z) = (u_*/\kappa)\ln(z/z_0), \tag{2.8}$$

where z_0 is the so-called *roughness height*. The resulting logarithmic velocity profile is shown in Figure 2.1. It is noteworthy, that the roughness height is not the average height of the bumps on the sea floor. Instead it is a fraction of it and represents a magnitude of the forces acting on the boundary surface (Grant and Madsen, 1986; Cushman-Roisin and Beckers, 2011). On the inner mud belt off Walvis Bay, Monteiro et al. (2005) determined a roughness height of $z_0 = 6.1 \times 10^{-4}$ m.

Now bringing together Equations (2.6) and (2.7), this leads to an expression for the TKE dissipation rate produced by shear turbulence ε_s in the near bottom layer,

$$\varepsilon_s = u_*^3/(\kappa z). \tag{2.9}$$

As we shall see later, the presented approach and assumptions can be very useful to estimate the TKE dissipation rate in the bottom boundary layer.

For a homogeneous and non-rotating fluid, the thickness of the bottom boundary layer would grow with time. However, if the Coriolis Effect and the effects of stratification are included in the theoretical approach, then the boundary layer is characterized by a limited thickness. Furthermore, the impact of rotation leads to the well-known *Ekman veering* of the horizontal flow in the near bottom layer. A comprehensive description and explanation on these topics can be found in Cushman-Roisin and Beckers (2011).

2.1.4 Turbulence in the stratified ocean

Mixing by turbulence generates vertical motions and overturning. In a homogeneous ocean, the required energy for mixing only has to be large enough to overcome mechanical friction. In a stratified ocean

however, where lighter water masses lie above denser ones, mixing involves the transfer of water across isopycnal surfaces of constant density. Therefore, turbulent eddies have to raise denser water masses above less dense water masses to overturn in a stratified ocean. Since work is being done against buoyancy forces, an increase in potential energy is required, which must be supplied by the kinetic energy of eddies (Thorpe, 2007).

Hence, the energetics of mixing in a stratified oceans differ from those in a homogeneous ocean, and the above defined Reynolds number no longer serves as a sufficient criterion for the onset of turbulence. Miles (1961) and Howard (1961) discovered that the instability of a steady, inviscid, two-dimensional, parallel, horizontal flow only appears, if the so-called *gradient Richardson number*,

$$Ri = \frac{N^2}{(du/dz)^2}, \tag{2.10}$$

is less than 0.25 somewhere in the flow, where du/dz is the vertical shear of the horizontal current $u(z)$. Variation of the vertical density gradient are expressed through the buoyancy (or Brunt-Väisälä) frequency N defined by

$$N = \sqrt{-\frac{g}{\rho_0}\frac{d\bar{\rho}}{dz}}, \tag{2.11}$$

where g is the gravitational acceleration, $\bar{\rho}$ the background density, and ρ_0 the constant reference density. The criterion $Ri < 0.25$ implies a necessary, but not sufficient condition for instability (Thorpe, 2007). On the other hand, flows in which Ri is greater than 0.25 are stable in a way that all small disturbances decay or propagate as internal waves without increase in amplitude.

The fact that the instability of a stable stratified shear flow is dependent on the Richardson number evokes that the local value of Ri could be used as a valuable guide to the elements leading to turbulence.

In addition to the previous numbers and quantities, a final measure is used in this thesis to evaluate turbulent characteristics. The vertical extent of a typical turbulent fluctuation is expressed by the *Thorpe length scale* L_T. The Thorpe length scale can be calculated from an observed instantaneous density profile, such as supplied by measurements of a CTD (conductivity, temperature, depth). The discrete density measurements from the instantaneous profile are monotonically rearranged to give a gravitationally stable profile. The vertical distance a fluid particle must be moved adiabatically in this process is its *Thorpe displacement* δ_T (Mater et al., 2013). The Thorpe length scale for a region is then given by

$$L_T = \langle \delta_T^2 \rangle^{1/2}, \tag{2.12}$$

which is the root-mean-square of all Thorpe displacements within a complete overturn (Gargett and Garner, 2008). In Chapter 4 of this thesis, the defined Thorpe length scale will be used to estimate the thickness of the turbulent bottom boundary layer.

2.2 Important mixing processes

A turbulent process can be defined as a physical mechanism. It is described by its effects and its associated spatial and temporal structure that generally involve the transfer of energy from one scale to another or from one part of the ocean to another. Although energy transfers from small to relatively large scales do appear in the ocean, the transfer of energy in the opposite direction down to very small scales is more substantial, since the smaller scales could be interpreted as turbulence (Thorpe, 2007).

The following paragraphs introduce the significant turbulent processes which are existent at the continental shelf of Namibia and may also influence the turbulent characteristics of the bottom boundary layer. Thus, they are relevant for this thesis.

2.2.1 Swell

Swell are barotropic surface gravity waves, accompanied by local currents and pressure fluctuations, which have been generated by wind fields far away and have travelled long distances over deep water beyond the area in which they are generated. For this reason, their direction of propagation is not necessarily the same as the local wind direction. While the waves travel very long distances, their energy is transferred from higher frequencies to lower frequencies. The resulting waves will have longer wave periods of 10 s to 20 s and typical wave lengths of 50 m to 150 m. Snodgrass et al. (1966) showed that swell can traverse entire ocean basins with very little loss of energy. Nevertheless, significant dissipation takes place in the bottom boundary layer of a shallow continental shelf (Herbers et al., 2000). In intermediate to shallow water (shallower than the surface wavelength of the swell), the influence of the bottom becomes significant, which is revealed by wave refraction, topographic scattering and dissipation of wave energy by bottom friction (Ardhuin et al., 2003). The characteristics of the swell can be described by the linear wave theory, which was first discussed by Airy (1845). Using the assumption that the wave height is infinitesimally smaller compared to the wave length and water depth, one can conclude that the surface waves comprise sinusoidal oscillations of the sea surface in space and time, which are accompanied by sub-surface currents describing an ellipse in the vertical plane of propagation. The ellipse tends to rectilinearity at the sea bed and the currents decrease downward.

According to the linear wave theory, the frequency of a gravity wave ω is given by,

$$\omega(k) = \sqrt{gk \tanh(kH)}, \tag{2.13}$$

whereby g stands for the gravitational acceleration, k for the horizontal wave number and H for the height of the fluid. Equation (2.13) is the dispersion relation, which links the wave frequency and wavenumber. The 'tanh' has two asymptotic values. In shallow water ($kH << 1$), the water depth is much smaller than the wavelength and $\tanh(kH)$ may be replaced by kH. Thus, the phase velocity c_p and group velocity c_g reduce to

$$c_p = \frac{\omega}{k} = \sqrt{gH} \quad \text{and} \quad c_g = \frac{\partial \omega}{\partial k} = \sqrt{gH}. \tag{2.14}$$

The group and the phase velocities are equal and independent from the wave number and thus the waves are non-dispersive. In contrast, in the case of deep water ($kH >> 1$), it follows that $\tanh(kH) \sim 1$, which leads to

$$c_p = \frac{\omega}{k} = \sqrt{\frac{g}{k}} \quad \text{and} \quad c_g = \frac{\partial \omega}{\partial k} = \frac{1}{2}\sqrt{\frac{g}{k}}. \tag{2.15}$$

In deep water, the group velocity is half of the phase velocity and the waves have a dispersive character. Thus, waves with longer wave length have greater phase velocities, which explains why the observed swell has relatively long periods compared to a local generated *wind sea*.

A further conclusion out of the linear wave theory is that the water level fluctuations of surface gravity waves are related to pressure fluctuations in the sub-surface layers. For an infinitely long wave, horizontal scales are much larger than the water depth, hence the water level is horizontal and the motions in the ocean are in *hydrostatic balance*,

$$p = \rho g H, \tag{2.16}$$

where ρ is the density of the water. However, for limited wave length the pressure fluctuations are smaller than $\rho g H$. The ration of the actual pressure fluctuations to $\rho g H$ is called the *pressure response factor* K_p (Kamphuis, 2010). It is a function of the wave length and the depth below the surface,

$$K_p = \frac{\cosh k(z+H)}{\cosh kH}, \tag{2.17}$$

where k is the wave number, H the depth and z the distance of a depth level from the sea surface. Equation (2.17) is very useful to determine the height of surface waves out of a pressure time series that

was gathered below the surface. Consequently, by obtaining the wave height, it is possible to calculate the wave power and thus, getting an impression of the intensity of the occurring swell. The wave power P is defined by Tucker and Pitt (2001) as

$$P = \frac{\rho g}{64\pi} H_s^2 T_z, \tag{2.18}$$

where H_s the significant wave height, which is the average of the highest third of the surface waves and T_z is the mean wave period. These quantities can be determined by a pressure time series by using the zero crossing analysis, which is explained in detail in the Subsection 3.2 (Kamphuis, 2010).

Coastal waters are typically shallow enough so that surface wave orbital velocities can be substantial at the bottom, which contribute to turbulence and mixing in the vicinity of the sea floor. Long waves with periods of 10, 14 and 20 seconds start to 'feel' the bottom approximately for depths of 50, 100 and 200 m, respectively (Huthnance, 1995). However, due to the short time scale of the wave, the oscillatory wave boundary layer, associated with shear stress of the wave motion close to the sea bed, extends only to a few centimetres above the bottom (Grant and Madsen, 1979, 1986; Brink, 2004). Nevertheless, past studies showed a strong monotonic decay of the swell energy between the shelf break and the shore region for high swell intensities at the North Carolina continental shelf (Herbers et al., 2000; Ardhuin et al., 2003). Hence, in this thesis the available high temporal data are used to investigate whether a similar impact of the swell on the near bottom turbulence is observable on the inner shelf off Walvis Bay.

2.2.2 Internal waves

Internal waves are gravity waves that travel within the interior of a fluid. They owe their existence to the stratified density structure of a fluid. An internal wave occurs at a sharp density change in the fluid along the interface. It comes with certain properties, e.g. the smaller the density contrast, the lower the wave frequency and the slower the propagation speed (Apel, 2002). Thus, internal waves have much lower frequencies and higher amplitudes than surface gravity waves, because the density differences within the ocean are usually much smaller than at the surface of the ocean. The maximum amplitude of an internal wave is at the density interface and its displacements are zero at the top and bottom of the water column, which gives it a baroclinic character.

In order to contribute to mixing of nutrients or to affect the mean flow of the ocean, these waves must become unstable, break and thus, produce turbulence. Processes, like shear instability, wave-wave interactions and topographic scattering transfer the energy of internal waves to smaller scales that eventually lead to dissipation (St. Laurent and Garrett, 2002). Often, instabilities and breaking of internal waves is observable in areas of steep topography (e.g., Klymak et al., 2012).

Internal waves are generally generated by two sources: alternating atmospheric wind forces near-inertial internal waves, while barotropic tides cause internal tides and non-linear internal waves (NLIW). In the case of relaxing wind, inertial motions develop in the oceanic surface mixed layer, which then propagate downward and excite inertial currents beneath the mixed layer. The rate, at which energy is transferred from the mixed layer to the interior, strongly depends on the horizontal scale of the mixed layer inertial currents and thus on the horizontal scales of the wind stress field (D'Asaro, 1985). Although the inertial motions produced in this way are most energetic in the mixed layer and upper thermocline, they extend throughout the ocean depth (Gill, 1984).

The most energetic internal waves are 'near-inertial' waves, with frequencies $\omega \approx f$, where the *Coriolis parameter* is defined by

$$f = 2\,\Omega \sin\phi, \tag{2.19}$$

where $\Omega = 2\pi/(\text{sidereal day}) = 7.292 \times 10^{-5}$ rad/s is the rotation of the Earth in fixed coordinates and ϕ the geographical latitude. On our rotating earth, the Coriolis force continually pulls moving particles at right angles to their velocity. In absence of friction or other external force, the water particles begin to move in a circle in an anticyclonic sense, with constant amplitude and period of $2\pi/f$. The path of

an inertial current repeats itself with time, so that inertial motions are also often referred to as *inertial oscillations*.

Nevertheless, wind-induced internal waves are not only generated by spatially variable and sporadic wind events (D'Asaro, 1985; Alford, 2001, 2003) that lead to inertial motions, but also by the regular and diurnal sea breeze effect (Lerczak et al., 2001; Miller et al., 2003). The sea breeze forces anticlockwise rotating diurnal variations of the current in the surface mixed layer and a reversed directed current beneath the thermocline, which balances the mass flux normal to the coastline in the surface layer and thus, leading to a baroclinic modal structure (Lass and Mohrholz, 2005). In the region of the critical latitude (30°S or 30°N), the near-resonant condition between local inertial and diurnal sea-breeze forcing can result in considerable vertical mixing on the continental shelf (Simpson et al., 2002; Zhang et al., 2009).

As mentioned before, tidal forcing also generates an internal wave field. *Barotropic tides* in the ocean are defined as periodic vertical or horizontal movements of the water particles, which are produced by variation in the gravitational field on the surface of the Earth, induced by the regular movements of the Earth-Moon and Sun-Earth systems. As a result of these multiple influences, many different tidal constituents develop, which means that the tidal energy is split among several frequency bands (Howarth and Pugh, 1983). However, since the shelf seas are frequently stratified by thermal and haline effects, there is consequently another class of tidal motions that may be excited through forcing of stratified flow over topography by the barotropic tide. These so-called *internal tides* are generated by carrying stratified water over the continental slope through the motion of barotropic tides. Figure 2.2 illustrates the underlying mechanism for a simple two-layer stratification on a continental shelf. During on-shelf barotropic tidal flow, the pycnocline is elevated in the vicinity of the shelf break by the positive and negative divergence of the flow in the top and bottom layers, respectively. Conversely, for off-shelf flow the pycnocline is depressed. This periodic forcing of the pycnocline results in internal waves of tidal frequency that propagate away into the deep ocean as well as onto the shelf (Simpson, 1998).

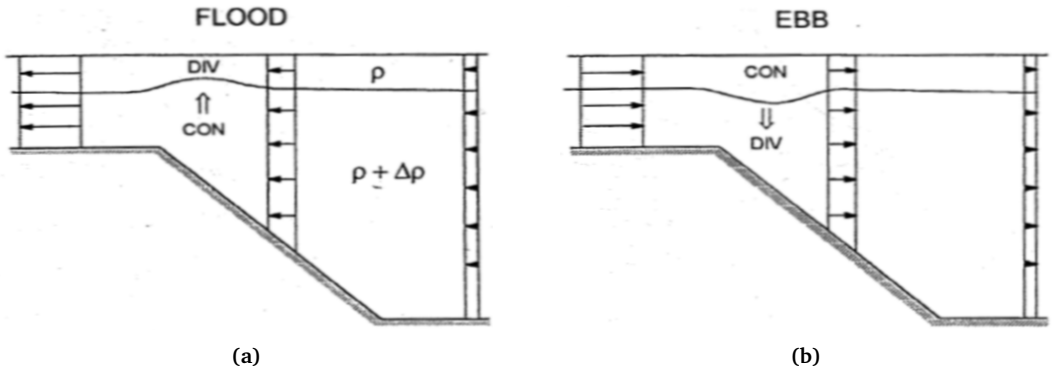

Figure 2.2: Generation of an internal tide due to barotropic stratified flow passing over steep topography at the shelf edge. The convergence and divergence in the cross-shelf flow forces the periodic vertical motion of the pycnocline. Taken from Simpson (1998).

Generally, the frequencies of internal waves cover a range from the local inertial frequency (f) to the buoyancy frequency (N), determined by the local stratification (Munk, 1981). At the limits, the internal waves degenerate to non-propagating oscillations, namely inertial and buoyancy oscillations, respectively (Olbers et al., 2012). If a stratified fluid is excited at a frequency greater than N, the fluid particles do not have the time to oscillate at their natural frequency and instead follow whatever displacements are forced on them (Cushman-Roisin and Beckers, 2011).

An interesting feature of internal waves is that for a continuously stratified ocean, the direction of the group velocity of an internal wave is inclined to the horizontal (Nash et al., 2004). Depending on their frequency, the wave energy spreads with a certain angle α, determined by the dispersion law of internal

gravity waves. The slope s of an internal wave beam is given by

$$s = \tan\alpha = \frac{k}{m} = \left(\frac{\omega^2 - f^2}{N^2 - \omega^2}\right)^{1/2}, \tag{2.20}$$

where α is the angle of the internal wave beam with respect to the horizontal plane. Subsequently, bottom slopes are classified by the ration γ/s, where γ is the topographic slope (Venayagamoorthy and Fringer, 2007). Slopes are considered to be subcritical $(\gamma/s < 1)$ when topographic slopes are flat compared to the wave characteristic slope, whereas supercritical slopes $(\gamma/s > 1)$ appear if the topographic slopes are steeper than the wave characteristic slope (Figure 2.3). Critical slopes $(\gamma/s = 1)$ correspond to waves in which the angle of propagation of the group velocity matches the topographic slope, leading to focusing of wave energy and increased amplitudes. Hence, non-linear effects become important and internal wave breaking occurs, leading to enhanced dissipation and mixing in the bottom boundary layer (St. Laurent and Garrett, 2002; Venayagamoorthy and Fringer, 2007; Lamb, 2014).

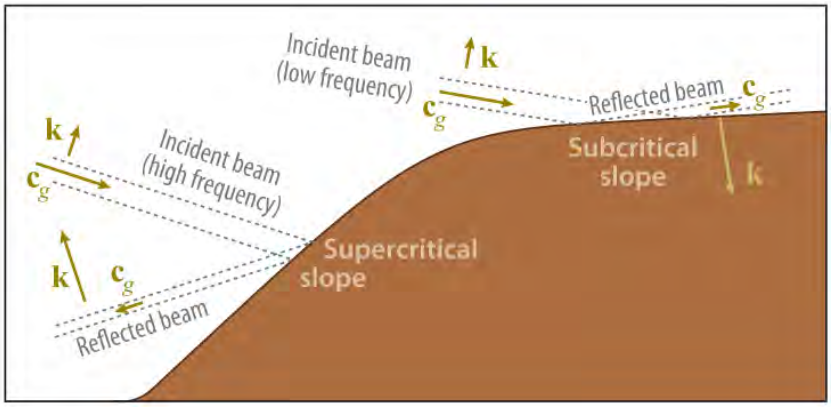

Figure 2.3: Reflection of internal wave beams from supercritical and subcritical slopes. Hereby, $\mathbf{c_g}$ is the group velocity, and $\mathbf{k}$ is the wave vector pointing in the direction of phase propagation of the internal wave. The reflected internal wave beams are narrower (i.e., shorter wavelengths) than the incident beams. Taken from Lamb (2014).

Non-linear internal waves

The description of internal waves by linear equations is only valid as long as the amplitude of the waves are small. However, in extreme cases, such as the interaction of internal waves with critical slopes, highly non-linear internal waves (NLIW) are generated. NLIW are ubiquitous wherever large tidal amplitudes and stratification occur in the neighbourhood of irregular topography (Apel, 2002). These waves do need not have tidal frequencies and are very energetic (Colosi et al., 2001). Their propagation carries considerable velocity shear that can contribute to turbulence and mixing in the ocean, which often introduces bottom nutrients into the water column, hence enriching the local region and reshaping the biology therein (e.g., Sandstrom and Elliott, 1984).

NLIW are non-sinusoidal isolated internal waves of complex shape with low wave dispersion that occur frequently in nature. For these reasons, they are also known as soliton-like waves or internal solitary waves in the literature. These waves are usually composed of several internal wave oscillations confined to a limited region of space. These given wave packets are generally characterized by dominant features: the individual oscillations are non-sinusoidal and depict predominantly downward displacements. Due to that, they are also described as *internal waves of depression*. Furthermore, Apel (2002) noted that the amplitudes of the individual oscillations are rank-ordered, with the largest at the front of the packet and the smallest at its rear; the wavelengths and the crest lengths are also rank-ordered, with the

longest waves again at the front of the group; and the number of individual oscillations within the packet increases as its age increases, with one new oscillation added per Brunt-Väisälä period.

Non-linear internal waves are widespread and observable in many coastal regions. In-situ observations of NLIW can be performed by using an ocean instrument capable of recording current, density or temperature. Due to the fact that they are coherent processes, these waves can also be recognized in photographs of the sea surface. These waves maintain their coherence and hence visibility through non-linear hydrodynamics and occur as long, quasi-linear stripes in imagery. The internal wave signatures are made visible by wave-current interactions in the surface layer. The velocity field in such waves induces a series of line convergences and divergences at the surface which, under conditions of light winds, locally modulate the surface height spectrum and thus, produce a pattern of alternating bands of rougher and calmer water spaced at intervals of 1-2 km, which can be observed visually in imagery (Simpson, 1998).

In recent decades, numerous studies observed NLIW in continental shelf regions and tried to find explanations of how they are generated (e.g., Sandstrom and Elliott, 1984; Holloway, 1983, 1987; Apel, 2002; Moum et al., 2003, 2007; Nash et al., 2004). These observational finding as well as numerical models of non-linear hydrodynamics (e.g., Klymak et al., 2012; Venayagamoorthy and Fringer, 2012) show that linear internal tides are transformed into non-linear baroclinic internal waves as they move up on the shelf. The determining process for the exact mechanism is still part of the scientific debate. Nevertheless, there is evidence that NLIW are either produced via lee wave formation, shear flow instability, or scattering of barotropic modes into internal baroclinic modes (Lamb, 2014).

NLIW are dissipated by radial spreading, bottom interactions, instability and fluid turbulence (Apel, 2002). Their strong currents result in instabilities in the bottom boundary layer beneath them, which are an important dissipation mechanism and an important source of sediment re-suspension (Sandstrom and Elliott, 1984). In the interior of the water column, shear instabilities in NLIW provide an important dissipation mechanism for the waves and result in significant vertical mixing of heat and nutrients (Lamb, 2014). Moreover, Nash et al. (2004) suspect that strengthened dissipation above the bottom near the critical slopes is related to enhanced shear in the internal wave field, rather than to classic bottom friction.

2.2.3 Continental shelf waves and coastal trapped waves

The last part of this chapter is devoted to low frequency wave motions that are trapped at the coast or over variable bottom topography.

In a coastal ocean with a flat bottom, geostrophic circulations are limited by the coast, which acts as a vertical lateral boundary. As a result, the coast prohibits flow across this boundary. Due to this absence of transverse motion, the fluid parcels are constrained to move in a vertical plane parallel to the lateral boundary. Thus, the horizontal alongshore component of the Coriolis force must vanish and consequently, a propagating barotropic wave is generated, which travels with the coast to the left on the southern hemisphere and to the right on the northern hemisphere. These waves are known as *Kelvin Waves*. Their amplitude falls of exponentially towards the open ocean in the order of the Rossby radius of deformation (Wang, 2002).

If now shelf topography is included to the system, another class of waves arise, the so-called *continental shelf waves* (CSW). These waves exist because of the presence of a sloping sea floor. On a rotating earth, the wind produces water movement in a surface Ekman layer, due to horizontal fictional stress (Cushman-Roisin and Beckers, 2011). The wind-driven horizontal transport in the Ekman layer is oriented perpendicular to the wind stress, to the right in the northern hemisphere and to the left in the southern hemisphere. If a shelf region is exposed to a periodically varying wind parallel to the coast, then this leads to periodic upwelling and downwelling at the coast and a compensating periodic onshore and offshore movement of the water column below the Ekman layer. As a consequence of the sloping sea floor and the conservation of potential vorticity, the onshore and offshore movement of the water column is associated with a continuous change of vorticity, which translates into the generation of propagat-

ing waves. These will leave the region of periodic wind forcing and will be observed as periodic water movement further along the coast, where the variations in the wind field are no longer related to them (Huthnance, 1981). These wave motions are known as continental shelf waves.

As well as Kelvin waves, CSW can only propagate with the coast to the left on the southern hemisphere and with the coast to the right on the northern hemisphere. They have similar periods as coastal Kelvin waves of several days to few weeks and similar wave lengths of the order of 2000 km, determined by the atmospheric weather patterns (Gill and Schumann, 1974; Huthnance, 1981). Nevertheless, CSW depict a different wave profile with a relative maximum of sea level oscillations over the shelf edge.

If the stratification of the shelf waters is taken into account, the shape of these coastal waves and associated currents are modified further, and so-called *coastal-trapped waves* (CTW) are generated. They also fluctuate on time scales of several days and propagate along the shelf and slope. Detailed information about CTW can be found in various literature, e.g. Gill and Clarke (1974), Brink (1991), Schumann and Brink (1990) and Kitade and Matsuyama (2000).

Chapter 3

Material and methods

The following chapter is intended to introduce the data used for the analysis and to present the methods. All analyses, calculations and plots have been performed by using the numerical computing environment MATLAB.

3.1 Hydrographic observations

The underlying data set of this thesis is composed of many different components, which are introduced and explained in the subsequent sections.

3.1.1 RV Mirabilis cruise MOM1301

The major part of the data used for this thesis was gathered during a cruise in January 2013 off the coast of Namibia. The RV Mirabilis cruise MOM1301 from 15 to 31 January was carried out as a joined cruise of the NatMIRC institute Swakopmund and three GENUS (Geochemistry and Ecology of the Namibian Upwelling System) project working groups. The major aim of the cruise was to contribute to the NatMIRC monitoring program and to lead to an improved understanding of the short term variability on the northern Namibian shelf.

Among other parts, the measurement program consisted of two transits along the 23°S monitoring line that covered the shelf, shelf break and partly the continental slope, beginning on 15 and 25 January, respectively. The transects at 23°S intersect the Walvis Bay upwelling cell and thus, they give information on the overall oceanographic situation on the shelf.

Between these measurements, a mooring with high temporal resolution instruments was deployed during the cruise, 20 nautical miles (nm) into the centre of the inner mud belt off Walvis Bay (23°S and 14°E), which was successfully recovered eight days later.

Simultaneously, ship-based measurements using a microstructure shear profiler (MSS), vessel mounted acoustic Doppler current profiler (VMADCP) and a CTD were conducted directly beside the mooring position to obtain a complete data set of high resolution hydrographic parameters in the whole water column.

CTD measurements

During the cruise, the CTD-system SBE 911+ (SEABIRD-ELECTRONICS, USA) was used to measure the following parameters: pressure, temperature, conductivity and oxygen concentration. This CTD encompasses a pumped system and a Rosette water sampler with ten Niskin bottles, each with a volume of five litres.

To avoid contamination of the CTD pumped system with air bubbles, the cast of each CTD measurement sets up at about 2 m depth below the sea surface. Subsequently, the instrument descends down to 800 m or 5 m above the bottom at shallower stations. The CTD collected data with a sampling rate of 24 Hz. The movement of the probe through the water column influences the water conditions. For this reason, the downcast was used exclusively for the data analysis. Nevertheless, water samples are taken on the upward profile in different depth levels, which build the foundation of many laboratory measurements on deck of the vessel.

After post-processing of CTD data, the residual errors for pressure, temperature, salinity and oxygen amount to 0.1 dbar, 0.004 K, 0.006 and 0.1 ml/l, respectively.

VMADCP measurements

A 75 kHz Vessel Mounted Acoustic Doppler Current Profiler (VMADCP), manufactured by RDInstruments, was mounted downward looking at the drop keel in 6 m below the water line. The ADCP measures with a frequency of 76.8 kHz and a beam angle of 30°. The gained data were combined online with the corresponding navigation data derived from vessel based GPS. The VMADCP was operated continuously during the entire cruise.

Post-processing of the VMADCP data was executed by using the MATLAB ADCP toolbox of IOW. The final profiles are 120 s averages of the single ping profiles of complex vectors for the horizontal velocity and a spatial vector for the vertical velocity. The residual errors add up to 3.44 cm/s. This observation method provides precise velocity measurements in the range of 24.5 to 104.5 m water depth which allows to analyse the currents in the interior water masses.

Microstructure profiler measurements

In addition to the standard CTD, a microstructure-turbulence profiler MSS 90-S was deployed at each station, in order to obtain information about turbulent mixing and stability of the water column. The microstructure-turbulence profiler (MSS) is a device to measure microstructure and precision of oceanic parameters at the same time. Two velocity microstructure shear sensors for turbulence measurements, a microstructure temperature sensor, standard CTD sensors for precision measurements, an oxygen sensor, a turbidity senor and a vibration control sensor are mounted at the head of the MSS profiler. The functionality of the shear sensors and details of the calculation of the physical shear from raw voltages are described e.g. in Prandke and Stips (1998). All sensors measured with a sampling frequency of 1024 samples per second. To reduce the impact of intermittency, three to five consecutive profiles were gathered at every station. Each set of profiles was averaged into a mean profile. After post-processing, the remaining errors for temperature, salinity and pressure amount to 0.004 K, 0.01 and 0.1 dbar, respectively.

The movement of profiler through the water column was conducted via a winch from the stern of the RV Mirabilis and the profiler was balanced with negative buoyancy, which results in a falling velocity of about 0.6 m/s of the profiler. Finally, a slack in the cable removed disturbing effects caused by possible vibrations and the ship's movement.

After gaining the measurements, the dissipation rate of turbulent kinetic energy (TKE) was determined by fitting the shear spectrum to the theoretical Nasmyth spectrum in a variable wave number range from 2 to a maximum of 30 cycles per metre (cpm). The limitation of the high wave number cut off is due to narrow band vibration peaks in the wave number range above 30 cpm, resulting from eddy generation at the probe guard of the profiler. The low wave number cut off at 2 cpm is used to remove any low frequent input from potential tumbling motions of the profiler (Nasmyth, 1970). Due to the intermittency of turbulence, this method requires repeated profiling to receive stable averages of statistical quantities. The free-falling microstructure probe exhibiting a typical noise level of $10^{-}9$ W/kg (Prandke and Stips, 1998).

3.1.2 Moorings

In order to obtain information about the temporal variability of hydrographic parameters on the inner shelf off Walvis Bay, two oceanographic moorings were deployed in 20 nm distance to the coast (23°00'S, 14°03'E) at about 130 m water depth (Figure 3.1). This location was mainly chosen due to three reasons: the mooring is located in the centre of the diatomic mud belt (Bremner, 1983), the sub-thermocline waters are oxygen depleted, and thirdly, this area is part of the convergence zone of SACW and ESACW (Mohrholz et al., 2008).

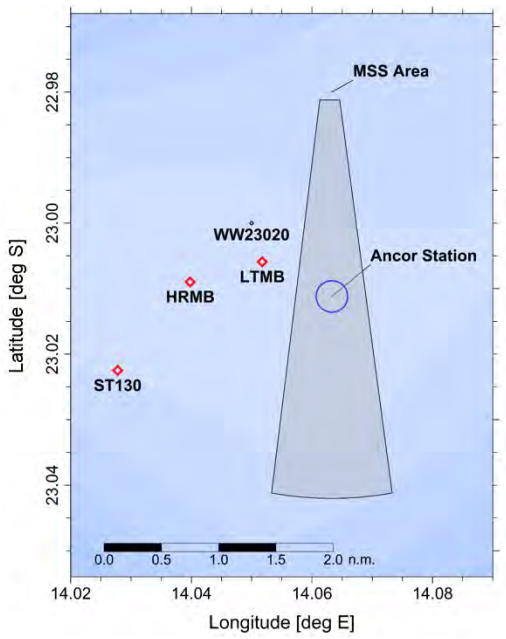

Figure 3.1: Detailed map of time series stations with the positions of moorings and ship-based measurements. HRMB and LTMB mark the positions of the corresponding moorings. The area shaded gray highlights the region where the ship-based CTD and MSS measurements were performed. Taken from Mohrholz et al. (2013).

The High Resolution at Mud Belt (HRMB) mooring was deployed on 17 January 2013 at 15:30 UTC at 23°00.539'S, 14°02.389'E and was successfully recovered on 25 January 2013 at 16:15 UTC. The main objective of this mooring was to obtain hydrographic data from the near surface and near bottom layer with a high temporal resolution. The high frequency data offer the possibility to analyse internal waves and other short term processes that control vertical mixing and re-suspension of suspended particulate matter (SPM).

The mooring consists of two Workhorse ADCP 600 kHz, three RBR TR1060 temperature recorders, and three RBR TRD2050 temperature pressure recorders (Figure 3.2(b)). Sadly no high resolution current measurements for the bottom layer are available, because the downward looking ADCP mounted in 40 m above the bottom broke down after 20 minutes of operation. Fortunately, every other instrument successfully accumulated data during the complete deployment period.

The purpose of the deployment was to observe transient processes on short times scales. Therefore, all instruments were set up to sample with maximum temporal resolution.

The Long-Term mooring on Mud Belt (LTMB) was deployed in November 2012 and was successfully redeployed in August 2013 after maintenance. The LTMB consists of an upward looking Workhorse ADCP 300 kHz, three MicroCat thermosalinometers SEB37, two SBE16 thermosalinometers with an Aanderaa optode for oxygen measurements, four RBR TR1060 temperature recoder, and one RBR DUO TDR temperature pressure recorder (Fig. 3.2(a)).

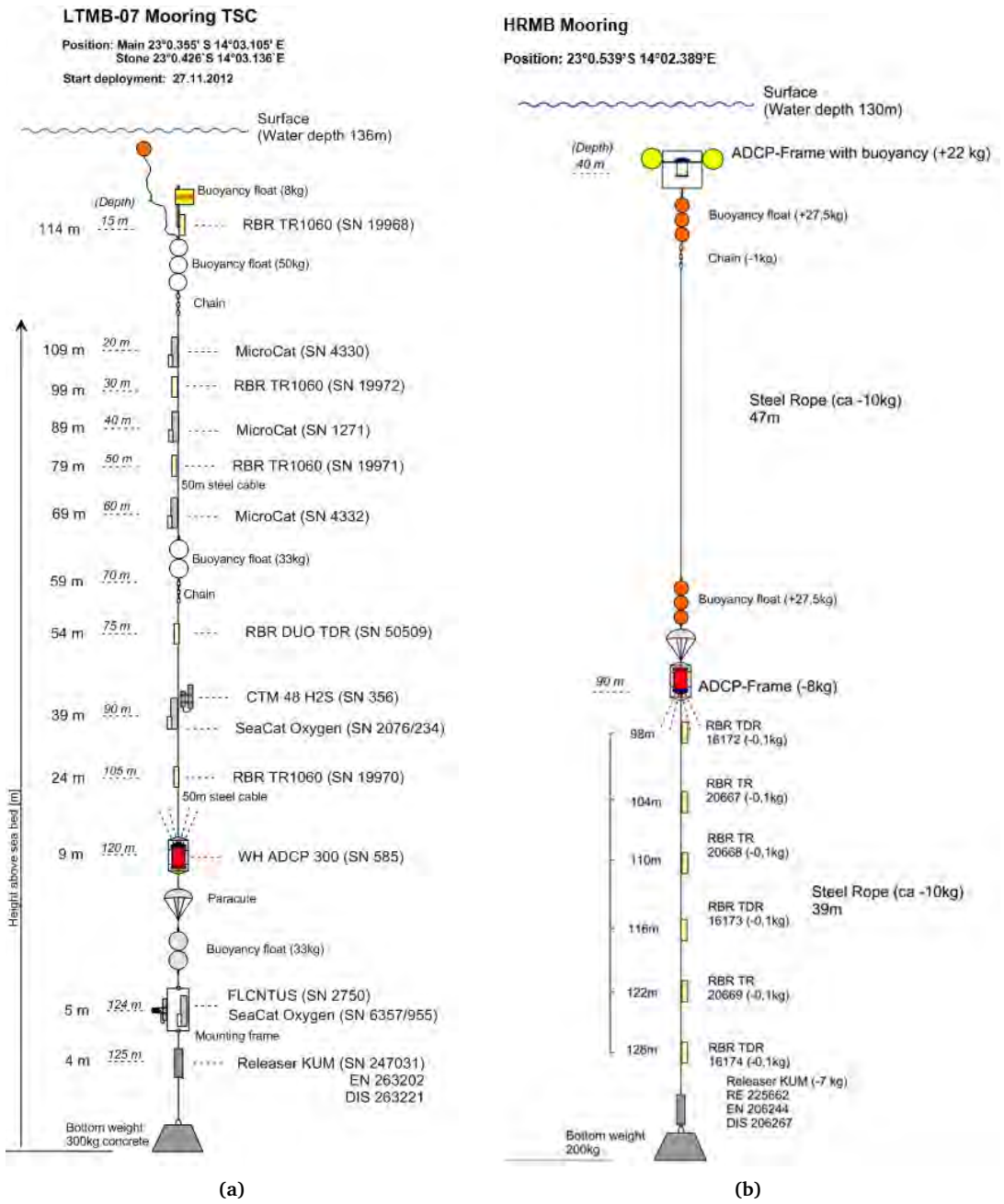

(a) **(b)**

Figure 3.2: Sketch of deployed moorings. The LTMB mooring is shown in (a) and the the HRMB mooring, which was deployed at the time series station during the cruise MOM1301 in (b). Taken from Mohrholz et al. (2011) and Mohrholz et al. (2013).

3.1.3 Remotely sensed data and weather observations

In order to put the observations at the mooring position in a larger perspective, satellite products were used. Remotely sensed daily sea surface temperatures (SSTs) are helpful in characterizing the intensity of the coastal upwelling during the cruise. Therefore, data was used from the GHRSST Level 4 SST analysis product on a daily basis and a spatial resolution of 6 km. The data can be accessed and more information can be obtained on the internet on the NASA website. [1]

In Chapter 4, moreover, a true color image from MODIS (Moderate Resolution Imaging Spectroradiometer) which is mounted on the Terra satellite, is used to observe internal solitary waves. A resolution

[1] http://thredds.jpl.nasa.gov/las/getUI.do

with a pixel size of 250 m was chosen. Daily images are accessible at the NASA website. [2]

Unfortunately, no weather station was mounted on the research vessel and thus, no weather information is available offshore. Nevertheless, hourly weather data could be downloaded for January 2013 from a weather station in Swakopmund close to the coast in an elevation of 21 m. [3] This data and the weather documentation in the cruise report (Mohrholz et al., 2013) are enough to get an idea of the prevailing meteorological conditions during the cruise in January 2013. The data is available with a temporal resolution of 5 min, but was averaged on hourly values for illustrative reasons.

3.2 Methods of analysis

The *zero-crossing method* is used to estimate wave characteristics out of a pressure time series. Individual waves can be determined by where the pressure crosses the mean level. Thus, the waves are characterized by a wave period, which is defined by where it crosses the mean level, and the wave height, which is defined by the distance from trough to crest between the crossings. As a result, one receives a wave record composed of many waves with a variety of heights and periods. Together with the correct pressure response factor (see Subsection 2.2.1), the pressure fluctuations can be transformed to elevations of the sea surface (Tucker and Pitt, 2001). If these waves are ranged by their height, the *significant wave height* (H_s) is defined as the mean of the highest third of all waves in the record. The *mean wave period* (T_z) is the mean of all periods in the ranking.

In order to determine the parameters H_s and T_z out of a pressure time series from the LTMB mooring, the Ocean Wave Analyzing Toolbox (OCEANLYZ) for MATLAB by (Karimpour, 2014) was used. Having that, it is finally possible to calculate the wave power of the swell (see Equation (2.18)).

Time series measurements of all oceanic parameters generally encompass fluctuations on various time scales and thus are generated by processes with different frequencies. For a detailed study of a particular process, filters are commonly applied to the data to separate low- and high-frequency components. Hence, unwanted frequencies can be eliminated while those of interest are emphasized. The Butterworth filter is a widely used method to high-, low- and band-pass filter diverse time series. Butterworth filters are characterized by a magnitude response that is maximally flat in the pass-band and monotonic overall (Wilcock, 2014). The amplitude spectrum of a Butterworth low pass filter is defined by

$$|G_{lowpass}(f)|^2 = \frac{1}{1 + \left(\frac{|f|}{f_c}\right)^{2n}}, \tag{3.1}$$

where f_c is the cutoff frequency and n is the order of the filter (Wilcock, 2014). Consecutively, the amplitude spectrum of a high-pass and band-pass filter is given by,

$$|G_{highpass}(f)| = 1 - |G_{lowpass}(f)|\,, \quad |G_{bandpass}(f)|^2 = \frac{1}{1 + \left(\frac{|f|-f_b}{f_c}\right)^{2n}}, \tag{3.2}$$

where f_b is the centre of the pass band and f_c here is the half width of the pass band. In this thesis, a digital fourth-order Butterworth filter was designed with a zero-phase digital response by processing the input data in both the forward and reverse direction.

Often, dynamical analyses require the separation of the tidal signal from sub or super-tidal variations in the time series of a measured parameter, such as pressure or currents. High-, low- or band-pass filtering techniques are generally useful to roughly split the tidal signal from residual fluctuations. Nevertheless, these are in most cases inefficient because adequately narrow filters with steep flanks are needed

[2] http://lance-modis.eosdis.nasa.gov/imagery/subsets/?subset=NBenguela
[3] http://other.weather.namsearch.com/swakop/wxwuhistory.php

(Pawlowicz et al., 2002). Furthermore, despite the filtering being beneficial in analyzing non-tidal fluctuations, it does not provide any information about the tidal characteristics. For this reason, functional methods, such as the *classical harmonic analysis*, have been devised by using the deterministic nature of tidal processes (Pawlowicz et al., 2002).

The classical harmonic analysis is based on the assumption that the astronomical forcing terms can be sufficiently described by a finite number of harmonic terms, each having different angular speeds (Howarth and Pugh, 1983). The tidal forcing is modelled as the sum of a finite set of sinusoids at specific frequencies. These frequencies are specified by numerous combinations of sums and differences of integer multiples of six fundamental frequencies originating from planetary motions (Godin, 1972). These fundamental parameters represent effects of the rotation of the earth (lunar day of 24.83 h), the orbit of the moon around the earth (lunar month of 27 days) as well as the earth around the sun (tropical year of 365.2425 days), and periodicities in the location of lunar perigee (8.847 years), lunar orbital tilt (18.613 years), and the sun's perigee (20,940 years). The set of six signed integers, required to specify a particular tidal frequency, is known as *Doodson numbers* (Pawlowicz et al., 2002).

In an equilibrium model, the response of the earth would be fast enough so that the surface deformation would effectively be in equilibrium with the forcing at all times. However, the relative slow speed of propagation of tidal waves in the deep ocean and the separation of the oceans through the continents both cause, that the real ocean is not in equilibrium with the tidal forcing. Nevertheless, as tidal amplitudes are small compared to the total ocean depth, the dynamics are nearly linear, implying that the forced response contains only those frequencies present in the forcing (Pawlowicz et al., 2002).

Accordingly, in the classical harmonic analysis, a tidal function is fitted to the observed data and the square of the residual difference between the model and the observed values gets minimised. The finite number of harmonic constituents used to obtain the tidal function depends on the length and quality of the observed data. In this thesis, 59 constituents were chosen for the analysis. In practice however, only a limited number of constituents contains most of the tidal energy and thus exceeding the chosen significance level of the *signal to noise ratio* (SNR) of 5. The harmonic analysis of current data (complex number notation) often uses the rotary components of the currents to additionally reveal the rotational characteristics of the current vectors and determine the sense of the rotations of the tidal constituent ellipse.

In this thesis, the classical harmonic analysis was performed by using a modified version of the *T_Tide* MATLAB toolbox (Pawlowicz et al., 2002). The analysis was carried out for gridded velocity data in complex vector notation on 46 depth levels. The temporal resolution of the grid was one hour and the vertical resolution 2 m between 20 m to 110 m depth.

Chapter 4

Results and analysis

4.1 Environmental conditions on the central Namibian shelf

The following section intends to describe the environmental conditions on the central Namibian shelf in January 2013, especially focusing on the eight-day period in which the high resolution measurements took place.

4.1.1 Meteorological conditions

As mentioned before, local weather conditions can essentially influence the hydrographical conditions of the coastal ocean. Figure 4.1 shows time series of hourly mean values of the following meteorological parameters: air pressure, air temperature, wind speed and wind direction from the station in Swakopmund, Namibia for January 2013. At first glance, it can be seen that the weather conditions were moderate and reveal no conspicuous extreme events.

The air pressure depicted a semidiurnal cycle, with moderate excursions around a mean value of 1014.0 hPa. The double peak in the daily pressure cycle is caused by solar thermal atmospheric tides (Whiteman and Bian, 1996).

The temperature time series shows a distinct diurnal cycle, as expected. The daily temperature fluctuates with a range of 3°C to 6°C. The monthly mean temperature in January 2013 was 19.2°C. However, from 12 January onwards, the time series describes a positive trend, which lasts until the end of the month.

During the time series station, moderate southwest trade winds prevailed. In January 2013, the wind blew with 3.0 m/s on average from westerly directions (258.7°). Some calm periods were observed. Like the temperatures, the wind depicts a diurnal variability, which is mainly due to the land-sea breeze effect. During the dark hours, the land cools down and calms or light northerly wind can be observed at the Walvis Bay region (Hart and Currie, 1960; Shannon and Nelson, 1996). As the day progresses, the solar radiation heats up the coastal area and the wind veers west and then south-south-west from which the sea-breeze develops just after noon (Figure 4.1).

The presented results are in agreement with the documentation in the cruise report (Mohrholz et al., 2013). Furthermore, it is mentioned that during nearly the entire time series station, a complete cloud cover or high fog layers prevented high solar radiation.

4.1.2 Sea surface temperature

Temporal and spatial development of sea-surface temperature (SST) is investigated, based on a Level 4 SST analysis product from the MODIS Terra sensor (see Subsection 3.1.3). The short-term variability of SST during the cruise is seen in high resolution satellite images in Figure 4.2. The SST is considered as

a proxy for the intensity of the Benguela upwelling. The observed structures illustrate the typical results of coastal upwelling off Namibia for austral summer months. The existence of packed isothermes, especially between Walvis Bay and Lüderitz and off Cape Frio indicates strong coastal upwelling in these areas. However, it is obvious that the SST increased from 17 to 25 January in the coastal area, indicating a weakening of the coastal upwelling. Particularly off Walvis Bay, the coastal upwelling reduced significantly during the observation period. The findings point to dropping southerly winds during those eight days.

Furthermore, mesoscale structures of cold water stretch seaward in a tongue-like shape with their origin in the coastal upwelling zone. These so-called filaments are particularly easy to identify seaward of the upwelling zone between Walvis Bay and Lüderitz. Near the coast inside the upwelling zones, the SST is around 17°C, compared to temperatures around 21°C at the surface of the open sea. Further North, at around 15°-17°S, Figure 4.2 clearly illustrates the existence of the Angola-Benguela frontal zone (ABFZ), where the equatorward flowing Benguela current converges with the poleward flowing Angola current and thus marks the northern boundary of the Benguela upwelling system.

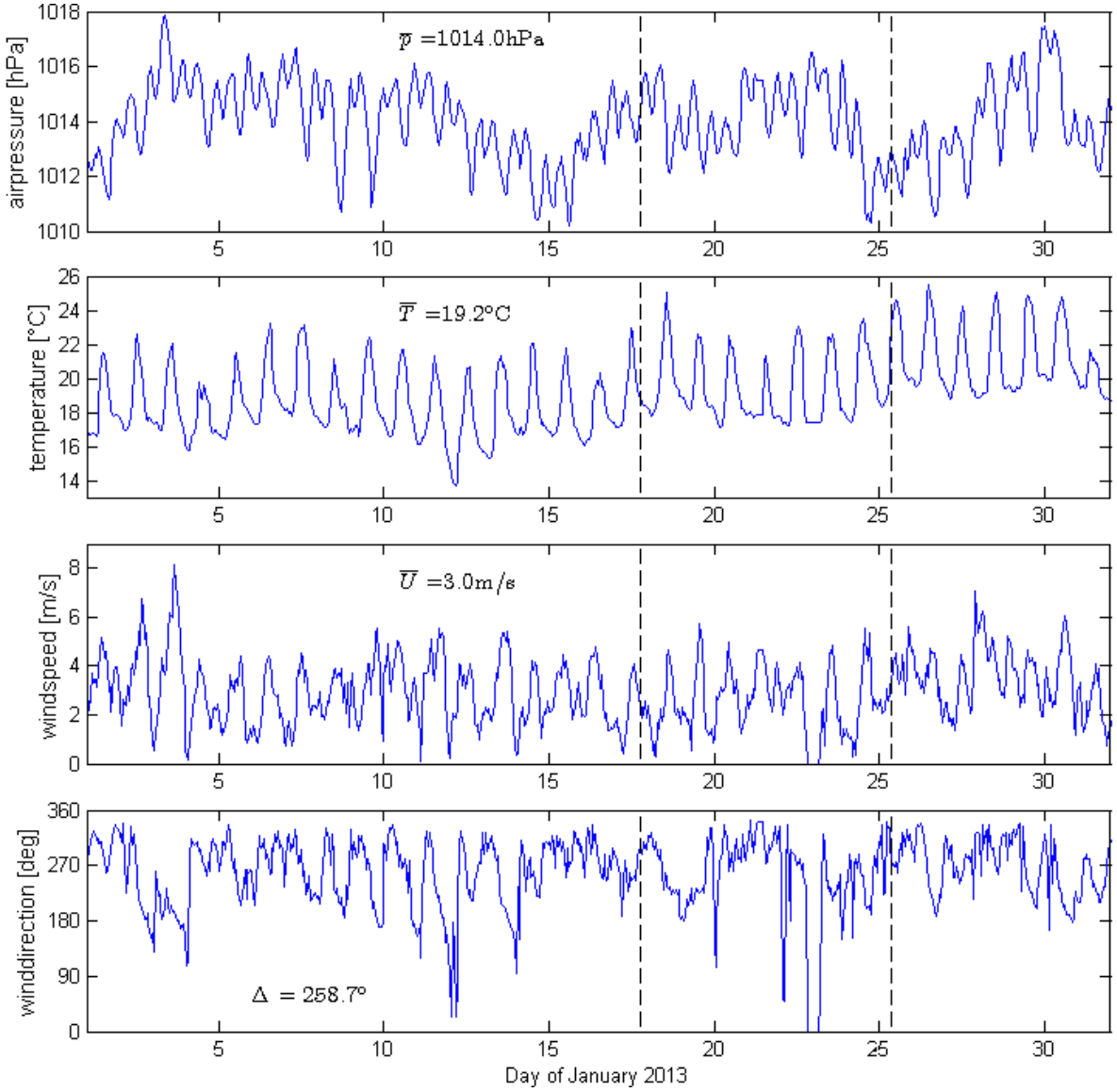

Figure 4.1: Hourly values of air pressure, air temperature, wind speed and wind direction from a weather station in Swakopmund in January 2013. The corresponding mean values for January 2013 are printed inside the plots. Information about the data are given in Section 3.2.

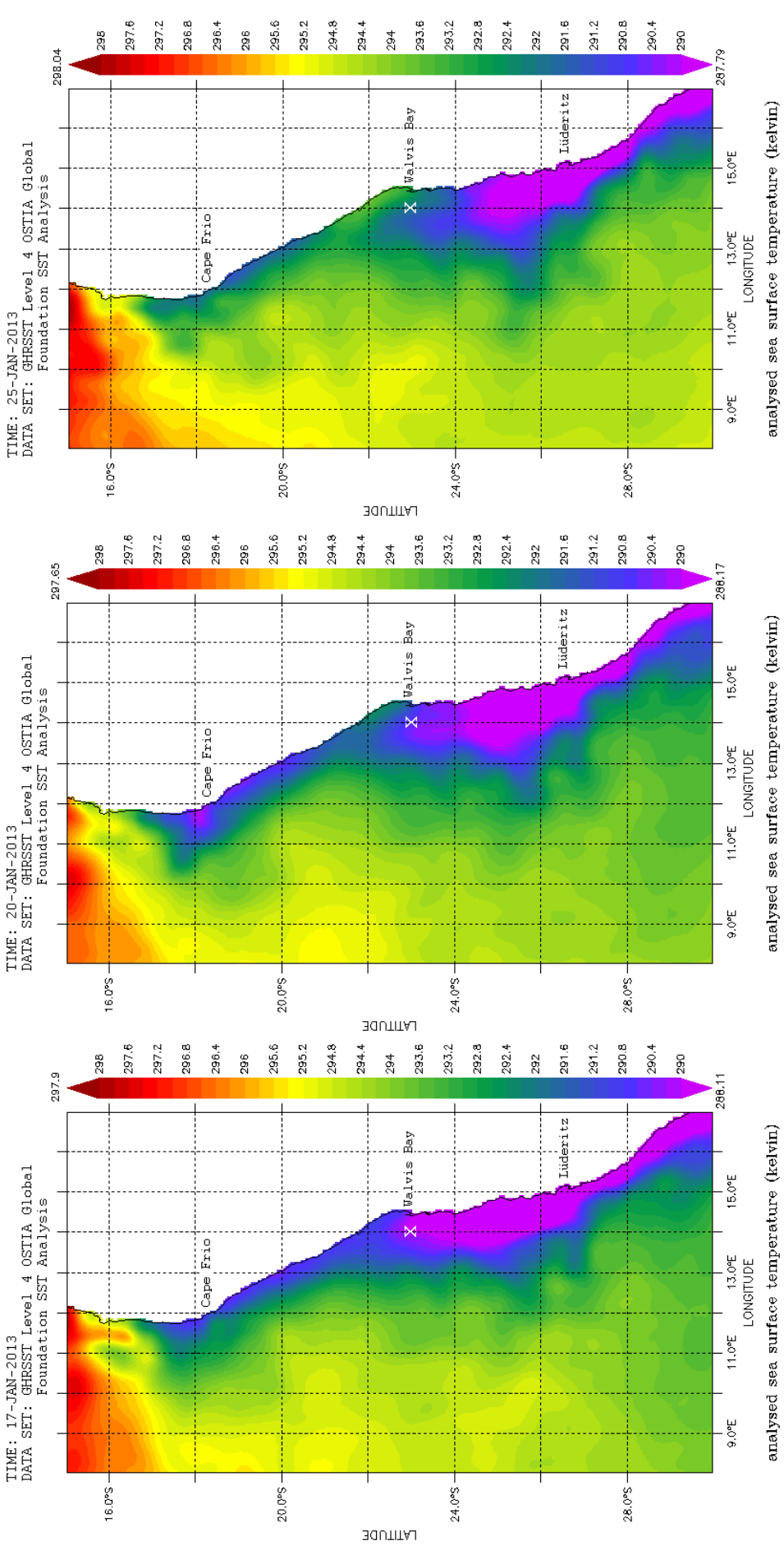

Figure 4.2: Distribution of sea surface temperature off Namibia based on GHRSST Level 4 OSTIA SST analysis from the MODIS Terra sensor. The spatial resolution is 6 km. The white cross marks the location where the moorings were deployed.

4.1.3 Transects along the 23°S line off Walvis Bay

The results of the CTD measurements along the 23°S line from 15 to 16 January and 25 to 26 January are shown in Figure 4.3. These zonal transects are helpful in spatially categorizing the mooring position on the inner shelf (14°E) in the hydrographical context on the continental shelf off Walvis Bay.

The shape of the shelf depicts a double shelf break, as already mentioned in the introduction. In addition, it is evident that the slope of the inner shelf region is only minimally tilted and especially inshore of the shelf breaks (13.6°S-14.0°S) the seafloor is nearly horizontal.

The observed thermohaline pattern in Figure 4.3 is exemplary for a cross shelf transect through an active coast upwelling cell in the northern Benguela. Only minor changes are observable between the two plots of the repeated transects.

Within the surface layer, temperature and salinity are decreasing from the offshore edge of the transect towards the coast from around 20°C to 17°C and 35.4 down to 35.1, respectively. The thermocline is very shallow (few tens of meters) above the shelf, where coastal upwelling occurs, and thickens significantly offshore the shelf break area (Figure 4.3). The temperature near the coast of around 14°C implies that the upwelled water originates from 100 m to 300 m depth.

The distribution of dissolved oxygen overlying shelf sediments in January 2013 (Figure 4.3(c)) confirms that bottom waters along 23°S were hypoxic or even anoxic during the observation period.

4.1.4 Temporal variability of hydrographic conditions

In order to investigate the temporal variability, time series for the entire water column from the CTD and MSS measurements are shown in Figure 4.4 and Figure 4.5 for the eight-day period in which the HRMB mooring was deployed. In total, 44 profiles and 86 averaged profiles were available from the CTD and the MSS measurements, respectively, to create the interpolated contour plots. Only minor changes are observable between the results of the two measurement methods.

The temperatures in the surface layer depict values around 17°C, with a daily increase up to 18°C from noon to the afternoon, when the solar radiation is at its maximum. Meanwhile, in the dark hours a cooling of the surface layer occurs. Temperatures decrease nearly linearly from the surface ($\sim$17°C) to the bottom ($\sim$12°C). The thermocline fluctuates around 20 m depth level with an excursion of roughly 10 m at a semidiurnal period, suggesting prevailing internal waves, namely the internal tides (Figure 4.4(a) and 4.5(a); Monteiro et al., 2005; Mohrholz et al., 2014). The vertical displacements of isotherms characterize the entire interior of the water column. The same behaviour is also displayed for the isohalines (Figures 4.4(b) and 4.5(b)) as well as in the time series of the dissolved oxygen (Figure 4.4(c)).

In the deeper part of the water column, colder temperatures and higher salinity can be identified between 19 and 22 January, whereas the latter half of the time series reveals increased values. These hint to a breakdown of the stratification in the near bottom layer from the middle to the end of the time period. Evidence for that can also be found when considering the temporal variability of the dissolved oxygen (Figure 4.4(c)). Anoxic conditions prevail in the near bottom layer for up to the last 25 m of the water column from the beginning up to 23 January. Afterwards, hypoxic conditions predominate close to the sea floor.

Salinity variability demonstrates a lower salinity in a subsurface layer in 20-40 m depth for the first half of the time series (Figures 4.4(b) and 4.5(b)). After 22 January, this feature disappeared. Certainly, the visible spatial and temporal variability of salinity should not be over-interpreted, due to the fact that the magnitude of salinity varies only in the small range of 35 to 35.2 in the whole water column and the entire period. If, finally, the distribution of dissolved oxygen is considered, it is obvious that the amount of dissolved oxygen decreases from the well ventilated surface layer ($\sim$5.5 ml/l) to very low values near the seafloor (between 0 to 0.5 ml/l).

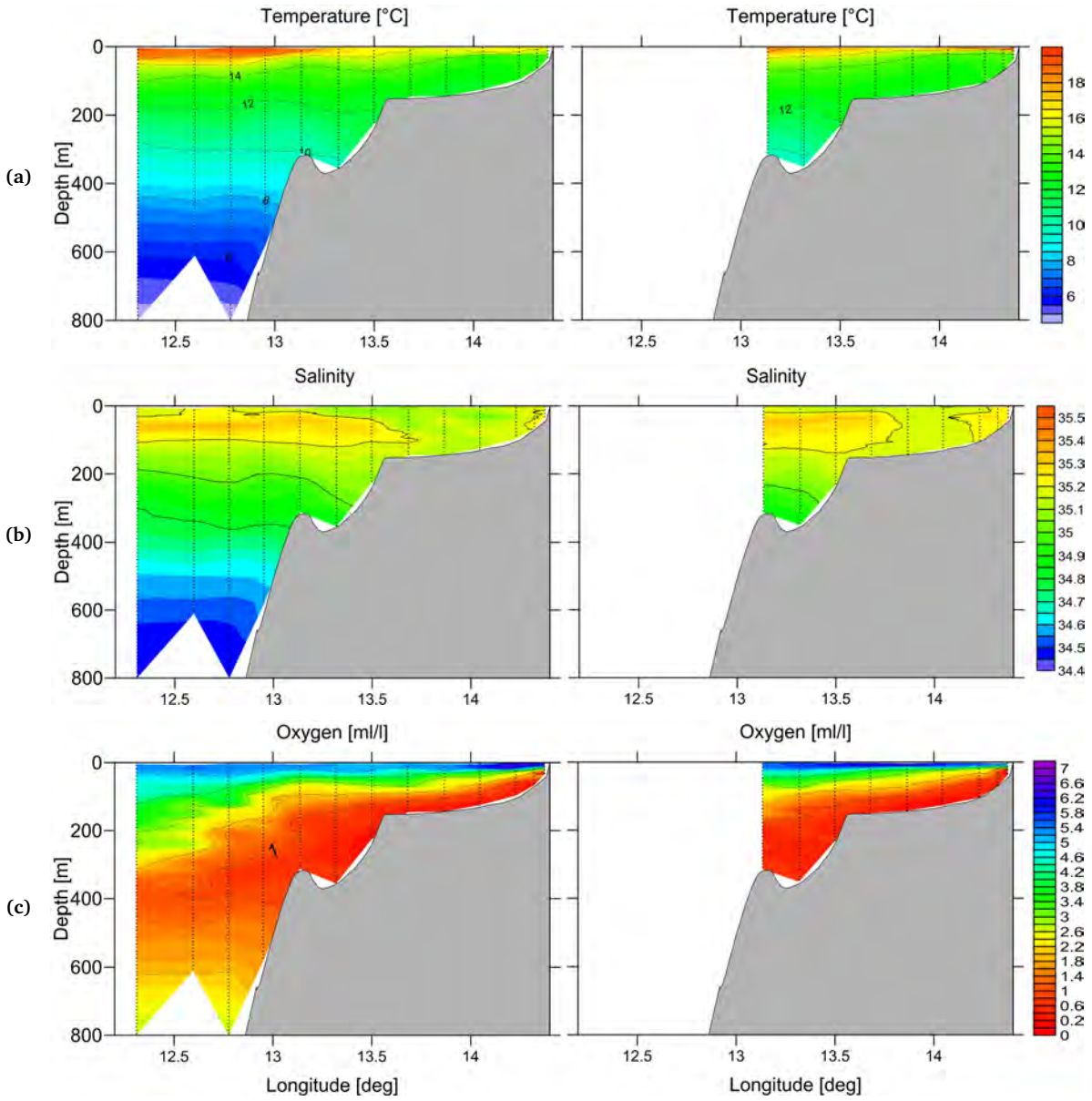

Figure 4.3: Distribution of temperature, salinity and oxygen concentration along the Walvis Bay transect for 15 to 16 January 2013 (left panels) and for 25 to 26 January 2013 (right panels). Taken from Mohrholz et al. (2013).

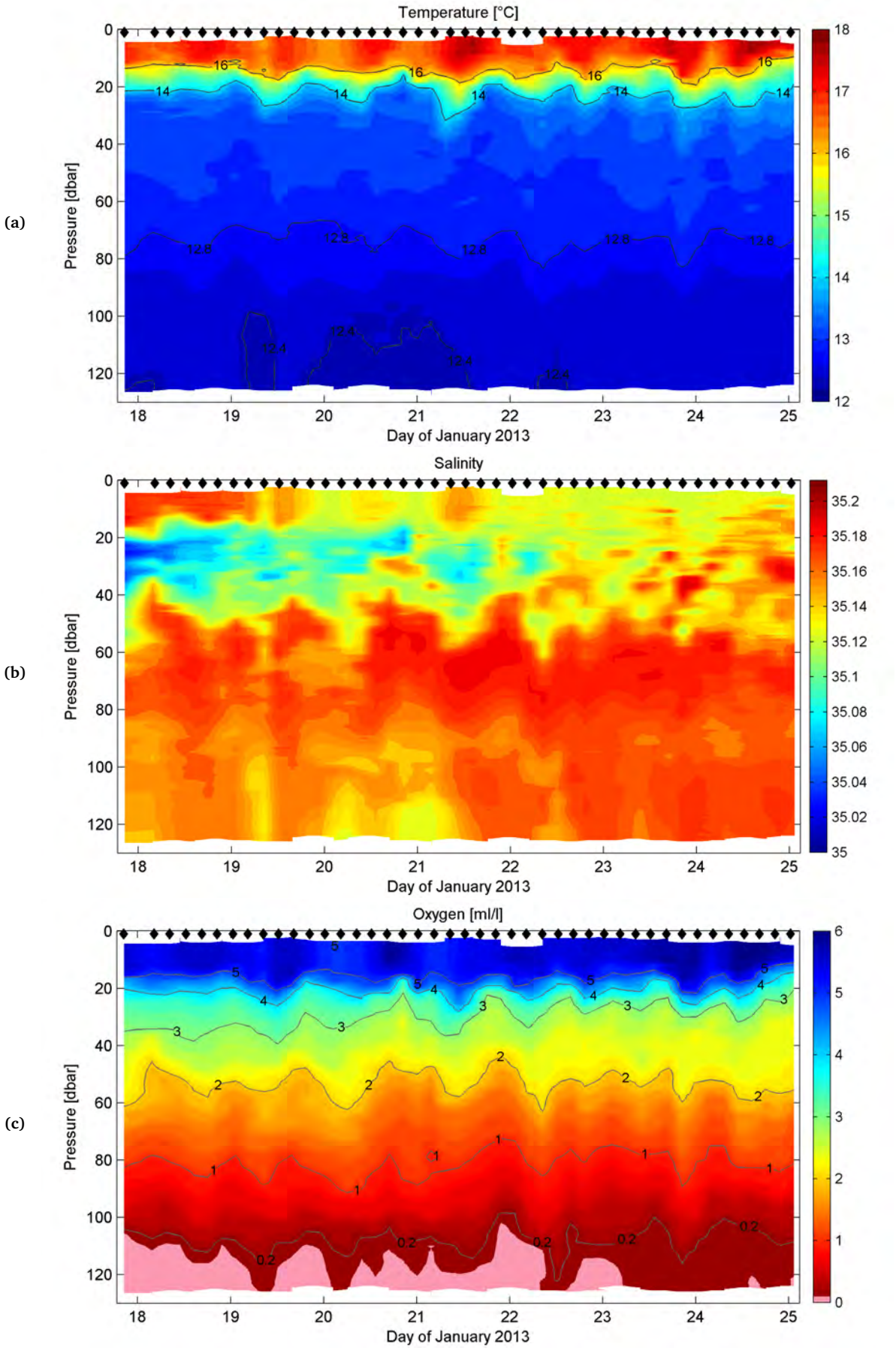

Figure 4.4: Time series of temperature, salinity and oxygen, gathered with a CTD probe on the inner shelf off Walvis Bay in the eight day period in January 2013. In total, 44 profiles with a vertical resolution of 0.5 dbar were linearly interpolated to obtain these contour plots.

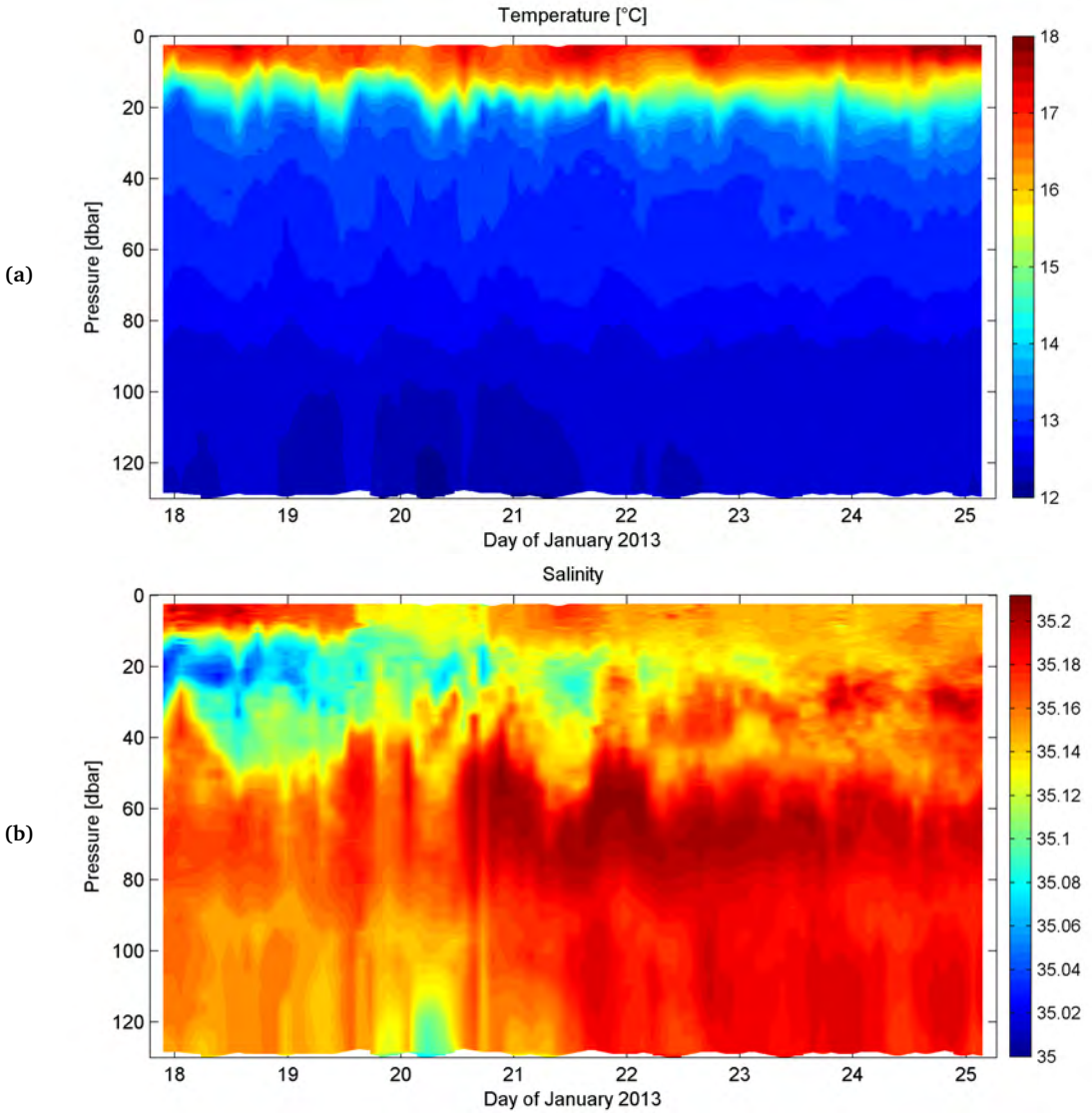

Figure 4.5: Time series of temperature and salinity gathered with the MSS on the inner shelf off Walvis Bay in the eight day period in January 2013. In total, 86 profiles with a vertical resolution of 0.5 dbar were linearly interpolated to obtain these contour plots.

4.1.5 Variability of near bottom temperatures

In the following, the results of the near bottom temperature time series, which were gathered using the HRMB mooring, shall be discussed (Figure 4.6). In total, six temperature sensors were deployed in the range of 98 m to 128 m depth and recorded the variability in temperatures with a sampling frequency of one second. Although the time series is too short for a spectral analysis, the visual inspection reveals fluctuations with periods from hours to a few days. It is noticeable that the high temporal fluctuations are significantly smaller in the time series of the two deepest sensors (122 m and 128 m). This behaviour points to a well mixed bottom boundary layer, which comprises at least the last 10 m of the water column.

The relatively large range of temperature values across the bottom layer (around 12.4°C in 98 m to 11.9°C in 128 m) between 19 and 21 January reveals that the water masses were well stratified in that short period. Afterwards, the stratification broke down and temperatures level off at around 12.4°C in the last 30 meters above the seafloor.

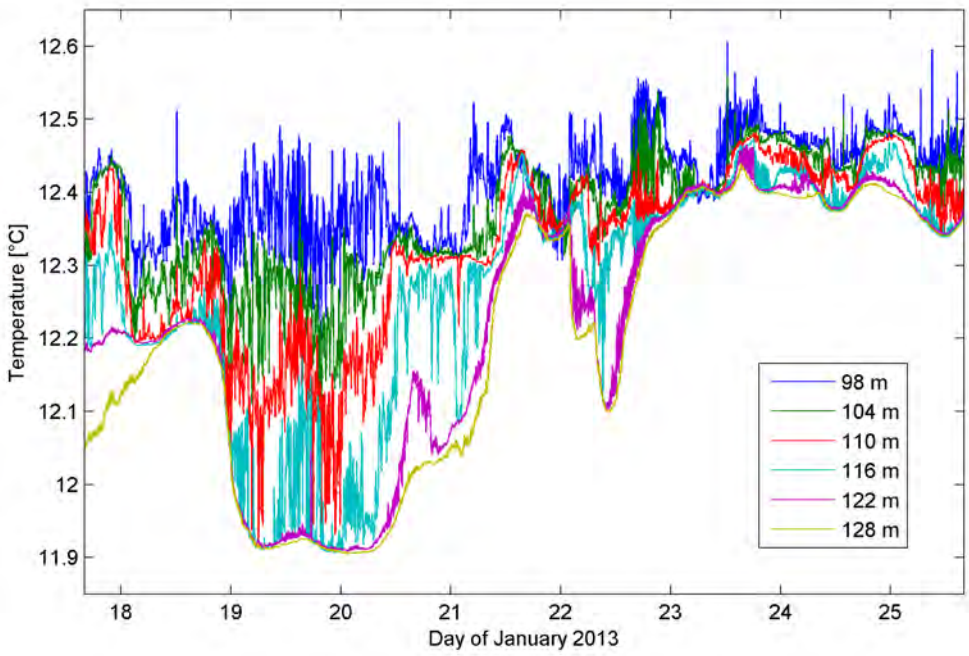

Figure 4.6: Time series of six temperatures sensors in the near bottom layer on the inner shelf off Walvis Bay in the eight day period in January 2013. The sensors recorded with a sampling frequency of one second.

4.2 Characteristics of turbulence in the near bottom layer

The overall aim of this thesis is to study the reasons for the variability of the near bottom turbulence. Based on this objective, it is appropriate to also have a look at the variability of the dissipation rate of the turbulent kinetic energy (TKE).

Figure 4.7 shows the time series of the TKE dissipation rate (ε) from the 60 m depth level to the sea floor. Values of ε vary on several orders of magnitude, from background values of around 10^{-9} W/kg to maximum values of 10^{-5} W/kg very close to the sea floor in 130 m depth. It is noticeable that the magnitude of ε is significantly larger in the near bottom layer in contrast to the values of ε in the interior of the water column, except for rare incidents of streaky structures with enhanced dissipation rates around the 90 m depth level are observable (Figure 4.7). These may be caused by sudden events of internal wave breaking.

The enhanced TKE dissipation rates near the bottom reach up to a maximum of about 25 m above the sea floor, but depict an intense temporal variability. Especially during the early hours of 18, 20 and 21 January and from 23 January onwards, low values of ε approach the seabed, resulting in reduced dissipation rates across the entire near bottom layer. On the other hand, relatively strong turbulence occurred in the night hours of 19, 21 and 22 January. Therefore, one can conclude that the turbulence in the near bottom layer depicts some variability on different time scales.

The open and motivating question now is: Which processes are responsible for the variability of ε in the near bottom layer? The path in search of an answer to this question will occupy the following part of this chapter.

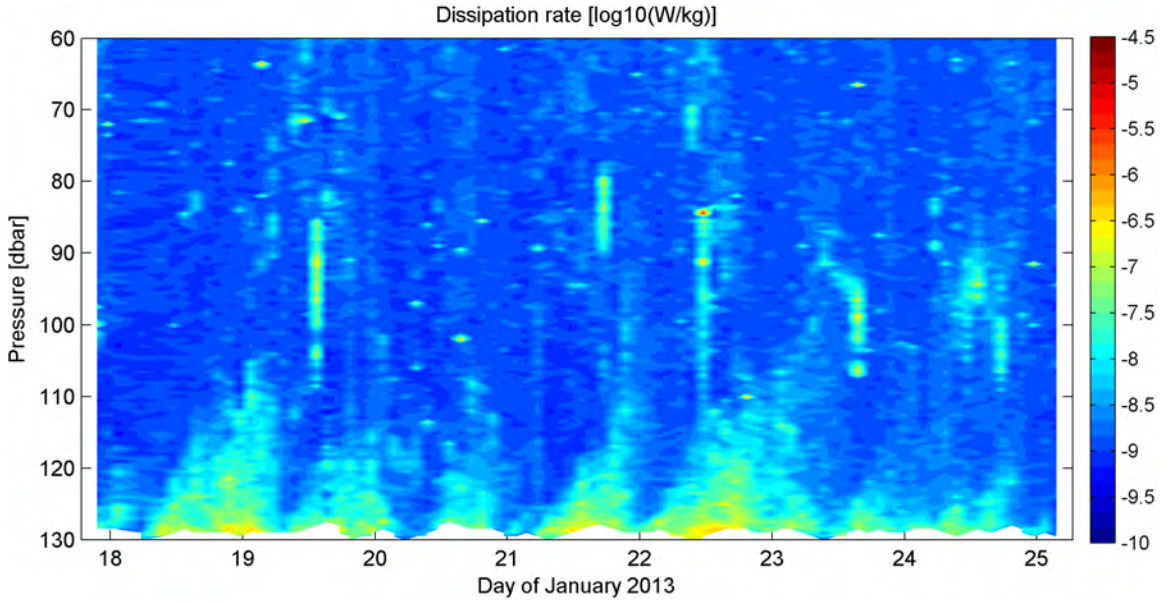

Figure 4.7: Time series of the TKE dissipation rate in the lower half of the water column measured by the MSS on the inner shelf.

4.3 Identification of significant dynamic processes

In order to get an overview of relevant processes that could have a possible impact on the turbulent mixing in the near bottom layer, two power spectra were calculated out of data from the LTMB mooring. Both data sets contain high temporal data from December 2012 to March 2013. The spectral analysis of the pressure time series in around 76.5 m depth and of the depth averaged horizontal current are shown in Figure 4.8 and Figure 4.9, respectively. The unit of the frequency axis is cycles per hour (cph). Generally, the power spectral analysis is a useful tool to identify the dominating processes and to investigate how the energy is distributed with respect to the frequencies of motion.

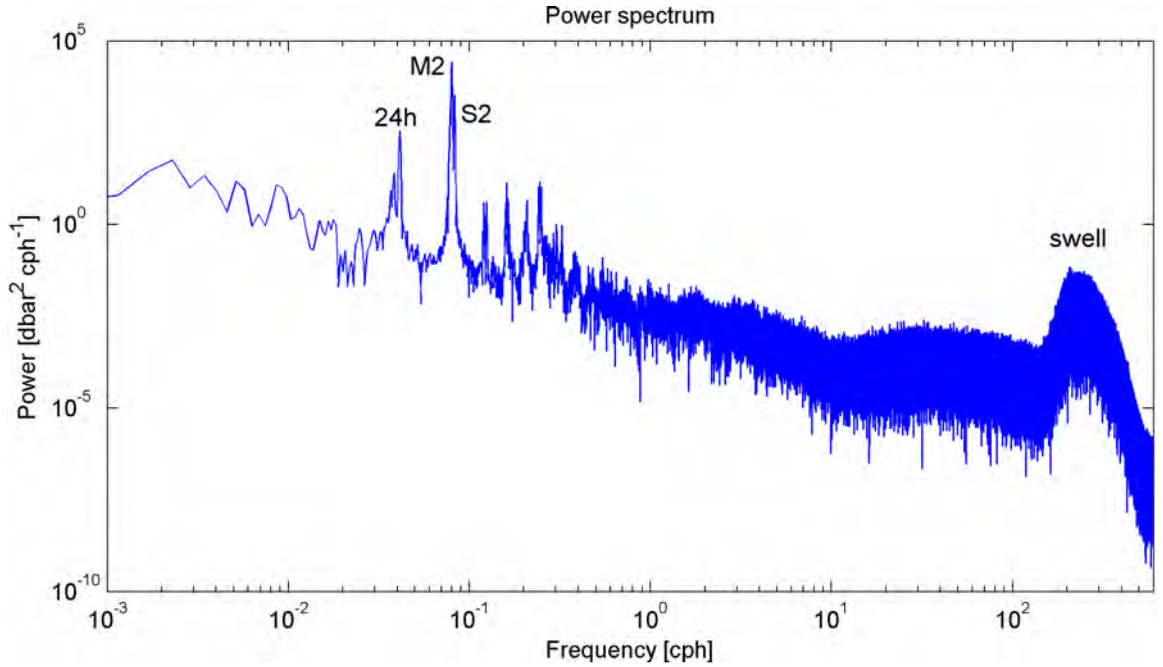

Figure 4.8: Power spectrum from the pressure time series in 76.5 m depth gathered with the LTMB mooring.

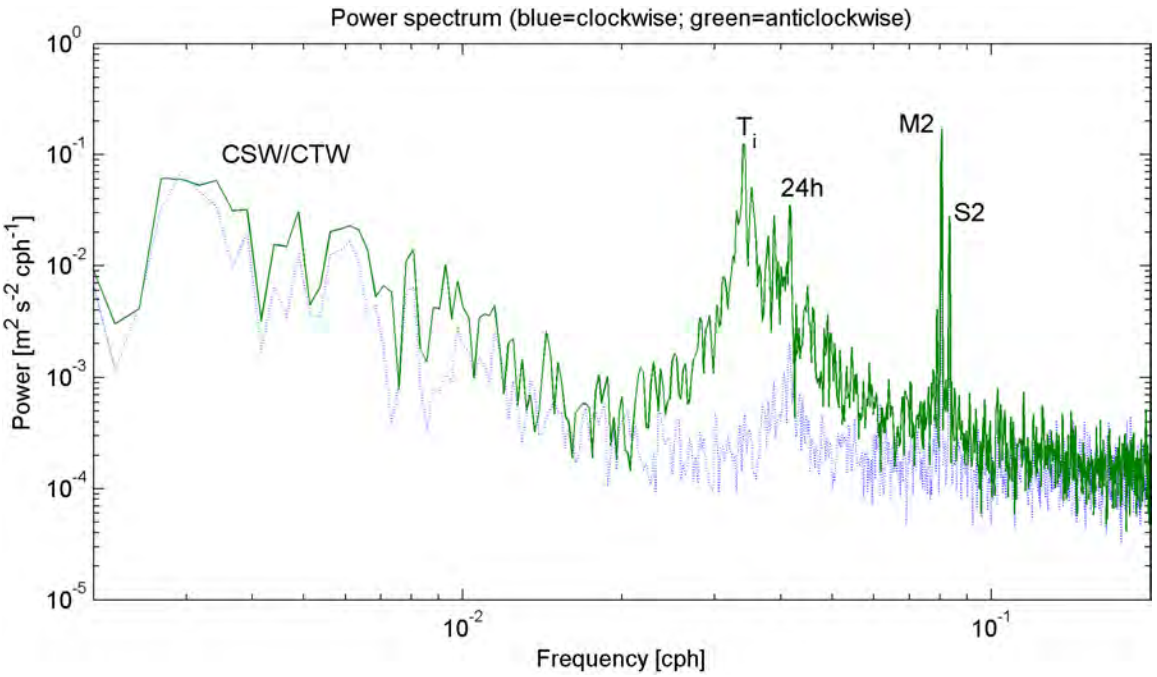

Figure 4.9: Power spectrum from time series of the vertical averaged horizontal velocities. Data was gathered with the LTMB mooring from 20 m to 110 m depth.

The spectral analysis of the pressure time series variability reveals that significant peaks occurred at semidiurnal tidal frequencies, around 24 hours and around 10 s to 20 s in the high frequency part of the spectrum (Figure 4.8). According to the time scales, the two latter ones are possibly generated by the diurnal sea-breeze effect (Rippeth et al., 2002; Lass and Mohrholz, 2005) and the swell, respectively.

A comparable outcome can certainly be observed in the second power spectrum, which was calculated out of the horizontal current time series (Figure 4.9). Due to the fact that the horizontal currents are given in complex notation, it is possible to derive rotary spectra, which additionally signal the direction of rotation of each outstanding process. This power spectrum also reveals high temporal variability over a broad frequency range. Again, powerful peaks stick out at the semidiurnal tidal frequencies and at the diurnal time scale. Supplementary and very energetic peaks are evident around the inertial period T_i, which is approximately 30.7 hours at the latitude of 23°S, and in the low frequency part of the spectrum. The latter peaks indicate the existence of CSW and CTW on the continental Namibian shelf (Lass and Mohrholz, 2005). Moreover, Figure 4.9 illustrates that the inertial and tidal motions are strongly polarised and reveal an anti-clockwise rotation. The direction of rotation results from the rotation of the earth and the location on the southern hemisphere.

The circular inertial motions, which are mainly generated by quick changes of wind at the sea surface (Knight et al., 2002), are not visible in the spectral analysis of the pressure fluctuations (Figure 4.9). This is very likely attributable to the accuracy of the pressure sensor, which is not sufficient enough to resolve the minor pressure fluctuations of the internal waves in around 76.5 m depth.

To gain more information about the oscillatory motions induced by tidal forcing, a classical harmonic analysis (see Section 3.2) of the current time series was performed to determine the significant tidal constituents. The results are presented in Table 4.1 and highlight that only three relevant tidal constituents (M2, S2 and N2) with semidiurnal frequencies are significant (SNR>5) on the central Namibian shelf. The calculated currents of the lunar semidiurnal tide (M2), solar semidiurnal tide (S2) and the large lunar elliptical tide (N2) are all within a few centimetres per second, whereby the M2 is the dominating constituent on the shelf off Walvis Bay. The corresponding tidal vectors rotate in the horizontal plane on an elliptical path, which is due to both the Earth's rotation and certain geographic conditions.

Table 4.1: Significant tidal constituents and their vertical averaged results (20 m to 110 m), determined by the classical harmonic analysis.

Constituent	Period [h]	Major axis [cm/s]	Minor axis [cm/s]	SNR
M2	12.42	2.99 ± 0.20	1.47 ± 0.18	140.01
S2	12.00	0.99 ± 0.20	0.57 ± 0.18	26.53
N2	12.66	0.51 ± 0.18	0.32 ± 0.17	8.99

4.4 Analysis of the swell variability

As mentioned before, this thesis is the first study on a possible impact of swell to the near bottom turbulence on the central Namibian shelf.

The swell was analysed by using the pressure time series of the LTMB mooring in 76.5 m depth (Figure 4.10(a), top sub-figure) from December 2012 to February 2013. This plot illustrates that the semidiurnal tides dominate the temporal variability of the pressure. The primary tidal constituents M2 and S2 differ slightly, which leads to a relative phase variation with a period of 14 days and is also well noticeable. Nevertheless, the object is to study the swell. For this reason, the high-frequency data has to be separated from the rest. For this purpose, a high-pass Butterworth filter of the forth order and a cut-off period of two minutes was used (see Section 3.2), so that only the fluctuations with periods shorter than two minutes are observable (Figure 4.10, second row). The obtained new time series already depicts an intensive temporal variability of fluctuations combined with alternating magnitudes.

If, furthermore, a spectral analysis is performed and the obtained power spectral density is displayed in a periodogram (Figure 4.10, third row), then several swell events are clearly detectable as small and tilted reddish areas. In a periodogram, the power spectral density is displayed as a function of the frequency and the time. It seems appropriate to identify the dominant periods and to localise the swell events. This plot perfectly illustrates that each swell event contains waves of different periods, whereby the waves with long periods propagate faster away from the area where they were generated and, thus, arrive earlier at the measurements location (explanation is given in Subsection 2.2.1). In addition, Figure 4.10(a) highlights that swell events are measurable on different time scales (from a few days to about one week), whereby each event shapes the surface wave field for a few days. Figure 4.10(a) also highlights that these events can coincide. Due to their dispersive character, swell events that originate from very far away, influence the dynamics for a longer time span, compared to events generated nearby.

Finally, the intensity of the swell events can be determined by calculating the wave power according to Section 3.2 (Figure 4.10(a), last row). The time series of the obtained wave powers is useful to evaluate the swell intensity for different time periods and thus, one is able to classify the results in an overall context.

The plots in Figure 4.10(b) represent a zoom into the relevant eight-day section of Figure 4.10(a), which is bounded by the dashed vertical lines. During that eight-day period, three swell events were detected at the mooring position, whereby the first two events are overlapping, which overall results in two broad peaks in the wave power with their highs around the 20 January and 23 January, respectively. Compared to other events in the three-month period in Figure 4.10(a), the intensity of the three swell events in the eight-day period is only moderate and lies around the mean level of the surface wave power from December 2012 to February 2013.

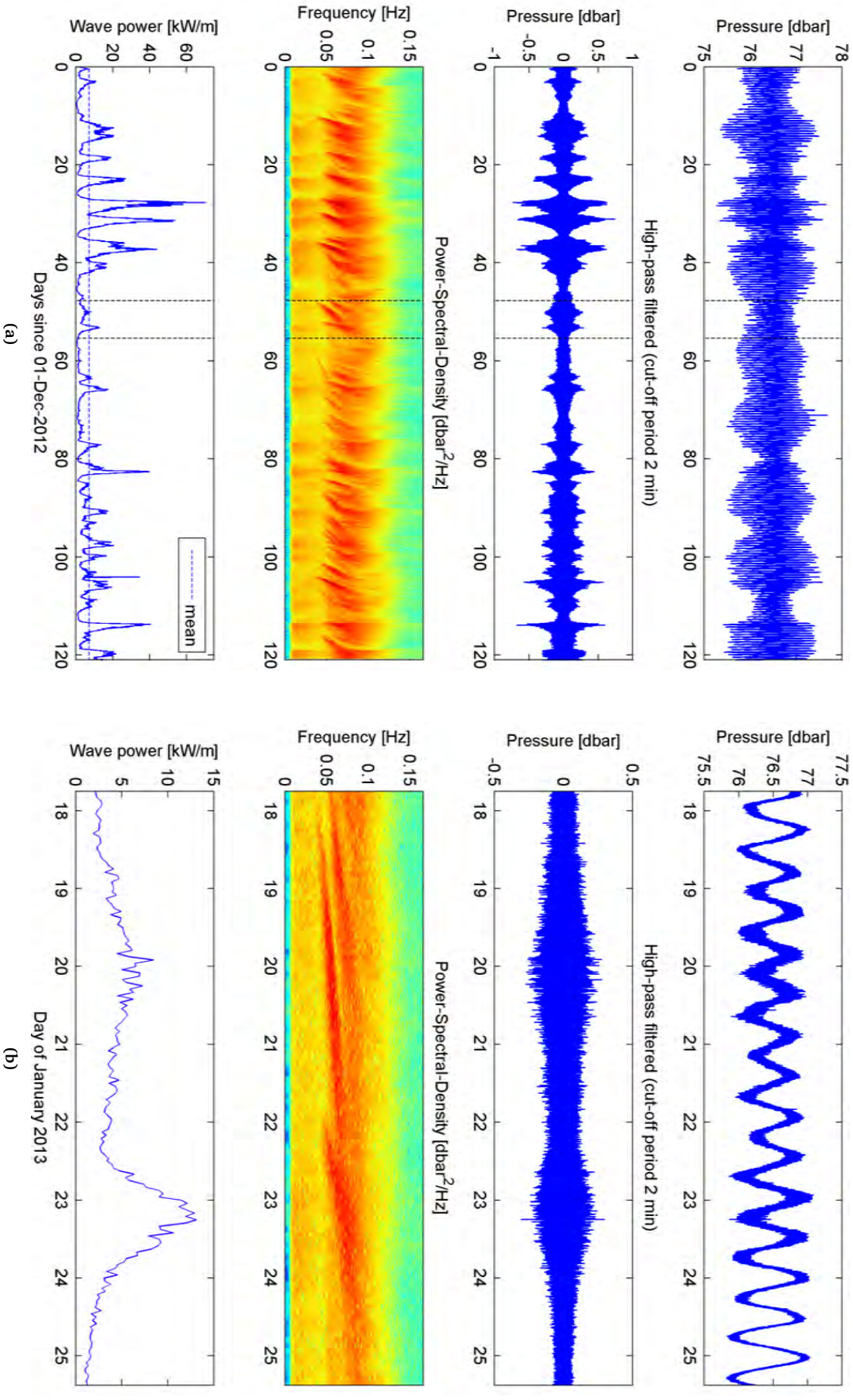

Figure 4.10: Observation and analysis of the swell in January 2013. From the top down, the individual rows illustrate: firstly the pressure time series in around 76.5 m depth, secondly the high-pass filtered pressure time series, thirdly the power-spectral density of the high-pass filtered time series and finally the calculated wave power of the surface waves. The right side (b) is a zoom into the section of the left side (a), which is bounded by the dashed vertical lines.

4.5 Study of non-linear internal waves

The characteristic properties and impact of non-linear internal waves (NLIW) have already been introduced in Subsection 2.2.2. Due to their baroclinic nature, they generate horizontal convergence and divergence in the surface layer, which influences the roughness of the ocean surface and, thus, are visible from space under clear sky conditions and during daylight.

Figure 4.12 shows a true colour image from the MODIS instrument on the Terra satellite (see Subsection 3.2) of the Namibian coast of 25 January 2013. The lower image is an enlargement of the previous one and clearly illustrates a package of shoreward propagating NLIW on the central Namibian shelf off the coast of Walvis Bay (signalled by the yellow arrow at the bottom of Figure 4.12). This proves the assumption made by Monteiro et al. (2005) that the NLIW are generated by the interaction of internal tides at the double shelf break of the central Namibian shelf.

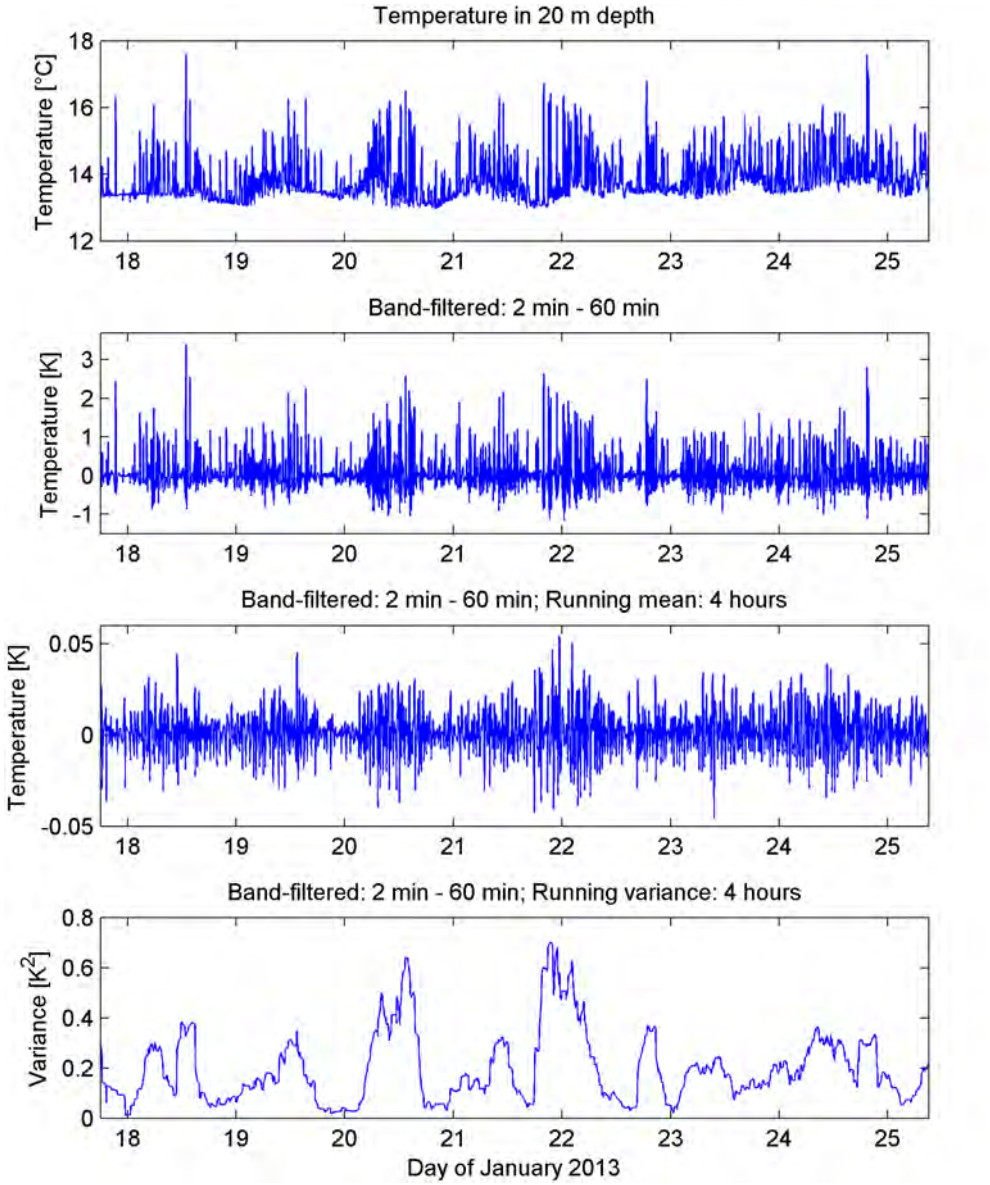

Figure 4.11: Different steps of the investigation of the variability of non-linear internal waves (NLIW). Starting from the temperature time series in 20 m depth gathered from a temperature recorder on the LTMB mooring with a temporal resolution of two minutes (top sub-figure). The following plots show the results for the band-pass filtered time series, the smoothed one by using a running mean and, further advanced, by using a running variance, respectively.

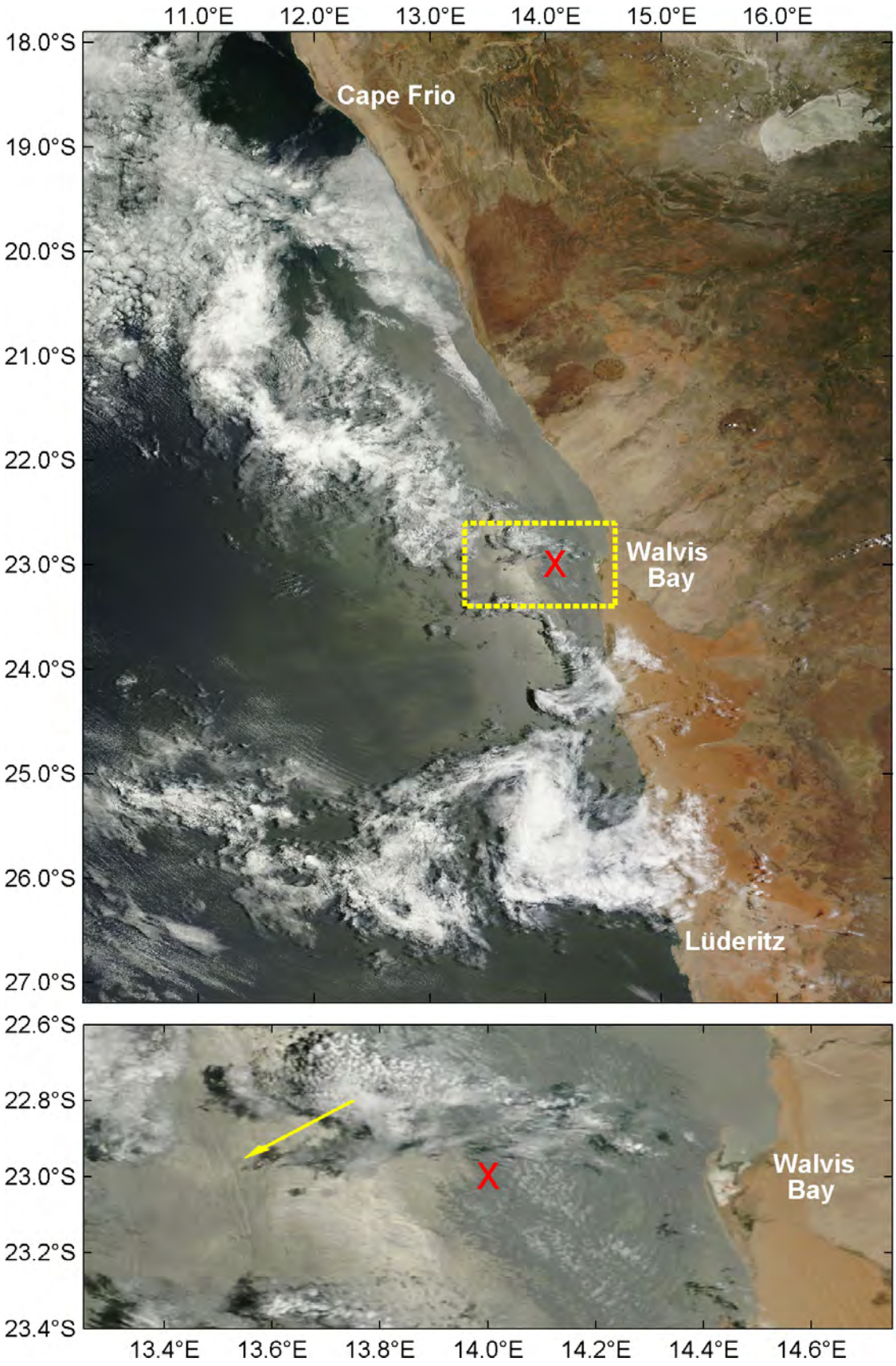

Figure 4.12: True color image of the Namibian coast from MODIS instrument taken on 25 January 2013. In both images, the locations of the moorings and ship-based high resolution measurements are marked with a red cross. The box with yellow dashed borders inside the top image indicates the area that is shown enlarged at the bottom. The yellow arrow points to a package of NLIW off the coast of Walvis Bay. The pixel size is 250 m.

NLIW are 'waves of depression', which means that they are linked to intensive downward vertical velocities in the interior of the ocean. As a consequence, temperature values at a certain sub-surface depth level increase while NLIW pass the stationary measurement. This property was used to investigate the temporal variability of this dynamic process. Due to the shape of the stratification on the inner shelf, temperature gradients are most pronounced at the depth level of around 20 m and thus, the temperature fluctuations are largest. For this reason, the temperature time series, measured with a temporal resolution of two minutes and mounted on the LTMB mooring in 20 m depth, was used for the investigation of the variability of the NLIW.

The different steps and the result of this analysis are shown in Figure 4.11. In the top sub-figure, the pure temperature time series is illustrated for the relevant eight-day period in January 2013. The mean temperature fluctuates between 13°C and 14°C on a diurnal time scale, but depicts countless upward outbreaks indicating quick temperature increases of up to 3°C and equally rapid returns back to the mean level. To investigate this behaviour in isolation and in more detail, the temperature time series was band-pass filtered with a lower cutoff period of two minutes and an upper cutoff period of 60 minutes using a Butterworth filter of fourth order (Figure 4.11, second sub-figure). These limits were chosen due to the reason that past studies pointed to periods of NLIW from 20 to 40 minutes (e.g., Apel, 2002; Nash et al., 2004; Monteiro et al., 2005; Lamb, 2014). The obtained time series elucidate the previous findings. The magnitude and frequency of the observable positive excursions of the temperature time series vary on a broad range of frequencies.

In the next step, the band-pass filtered time series was smoothed by using a running mean with an averaging period of four hours (Figure 4.11, third sub-figure). This was necessary to emphasize the periods where a large number of energetic NLIW passed the mooring in a relatively short time and thus, indicating times of great NLIW intensity.

Finally, to carry this approach to a meaningful and understandable result, a running variance with a computation period of four hours is performed on the processed time series. The outcome is shown in the last sub-figure of Figure 4.11 and simply depicts the temporal variability and intensity of the NLIW for the eight-day period in January 2013.

The most pronounced intensities are observable in the daylight hours of 20 January and in the night hours of 22 January. Somehow indistinct, almost daily peaks occur, although intensity and interval between the respective maximum values fluctuate considerably. Nevertheless, these findings indicate the complexity of the NLIW.

The analysis of the variability and properties of the NLIW is completed by the inspection of the vertical velocities from the upward looking ADCP mounted in 40 m depth on the HRMB mooring. Figure 4.13 illustrates the effects in the vertical velocity in the sub-surface layer while several NLIW of different intensity are passing by the moored instrument. The represented time section for 19 January from 8:30 UTC to 14:30 UTC, shows the passage of at least five internal waves and reveals some of the major characteristics. The downward vertical velocity ahead of the wave and subsequent upward velocity following the wave indicted the internal fluid motion resulting from the passages of the NLIW in their form as waves of depression. The first half of each wave depicts strong downward directed velocities of around 1 cm/s to 4.5 cm/s. After a some minutes, the motion reverses and strong upward directed velocities of the same order are observable.

In addition, the vertical velocities decrease towards the sea surface, indicating the baroclinic nature of the internal waves, where the vertical velocities have to be zero at each, top and bottom boundaries. Unfortunately, due to the tilted position of the ADCP on the mooring, no current data is available in the top ten metres of the water column to clarify the previous findings.

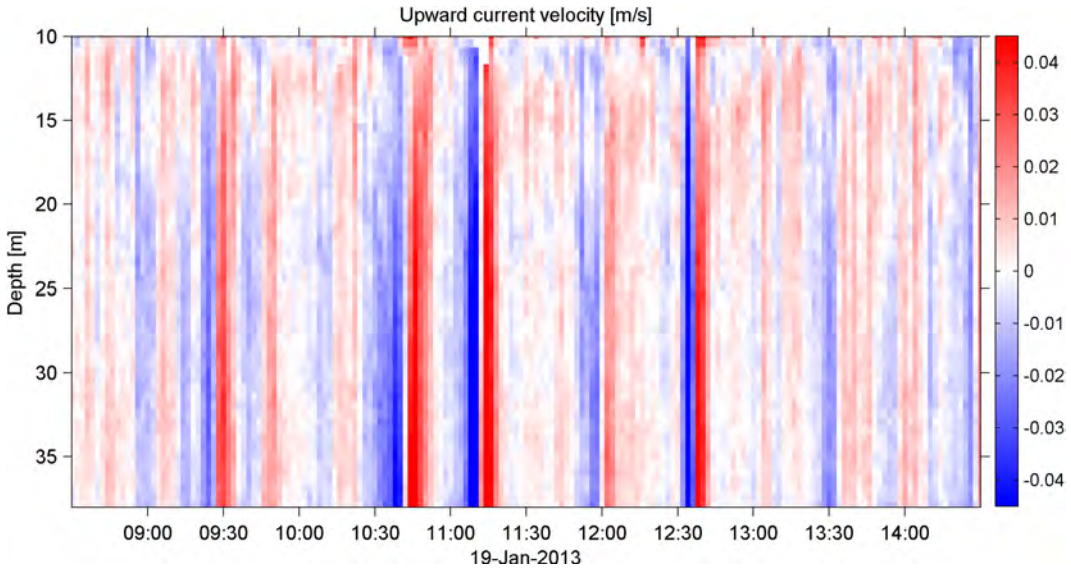

Figure 4.13: Six hour section from 19 January of the vertical velocity measured by the upward looking ADCP mounted on the HRMB mooring.

4.6 Turbulence caused by bed shear stress

The last process that is investigated in detail in this thesis is shear-induced turbulence in the bottom boundary layer. As mentioned before, unfortunately, no direct measurements of the currents in the near bottom layer are available, because the downward looking ADCP of the HRMB mooring stopped working immediately after deployment. Nevertheless, there is some velocity data available from the VMADCP from the ship-based measurements for the relevant eight-day period in January 2013. These data is obtainable down to the 104.5 m depth level. At this level, the horizontal current (not shown) has a mean value of 7.2 cm/s and a maximum of 16.1 cm/s during the eight-day period.

If one now assumes that according to Equation (2.8) (see Subsection 2.1.3), the vertical profile of the horizontal velocity in the near bottom layer has a logarithmic shape and additionally uses the deepest available horizontal current value as a base point, then it is possible to estimate the currents in the near bottom layer. This approach was successfully realised. By taking the estimated velocity profile, subsequently, quantities like the TKE dissipation rate ε_s from the shear stress can be determined by using Equation (2.9), and the magnitude of the bed shear stress τ_b can be calculated by using Equation (2.6).

A justification for this approach is provided by analysing the Thorpe length scale L_T in the near bottom layer (Figure 4.14; also see Subsection 2.1.4). The Thorpe length scale expresses the vertical extent of a turbulent fluctuation at a certain point in the water column and thus, indicating the vertical extent of the bottom boundary layer. Here, L_T was calculated by using the density profiles, which were obtained from the CTD data of the microstructure profiler measurements. Enhanced values of L_T with maximum values of 28 m are observable in the bottom boundary layer. Fortunately, apart from a few outliers in both directions, the increased Thorpe length scales approximately extend to the 105 m depth level in the observed eight-day period in January 2013 (Figure 4.14). So it is justified to take the magnitude of the measured horizontal velocity in 104.5 m as the base point for the estimation of the velocity profile in the near bottom layer.

The gradient Richardson number Ri has already been introduced in Subsection 2.1.4 as a criterion for the onset of turbulence in a stratified fluid. Figure 4.15 illustrates the time series of Ri in the lower half of the water column on the inner shelf off Walvis Bay during the eight-day period in January 2013. Very small values of Ri can be found within a few metres above the seafloor, indicating that at those depth levels, the vertical shear of the horizontal currents dominates over the stratification effect thus leading to turbulent conditions. However, the height of the isoline of the criterion $Ri = 1/4$ varies from a minimum

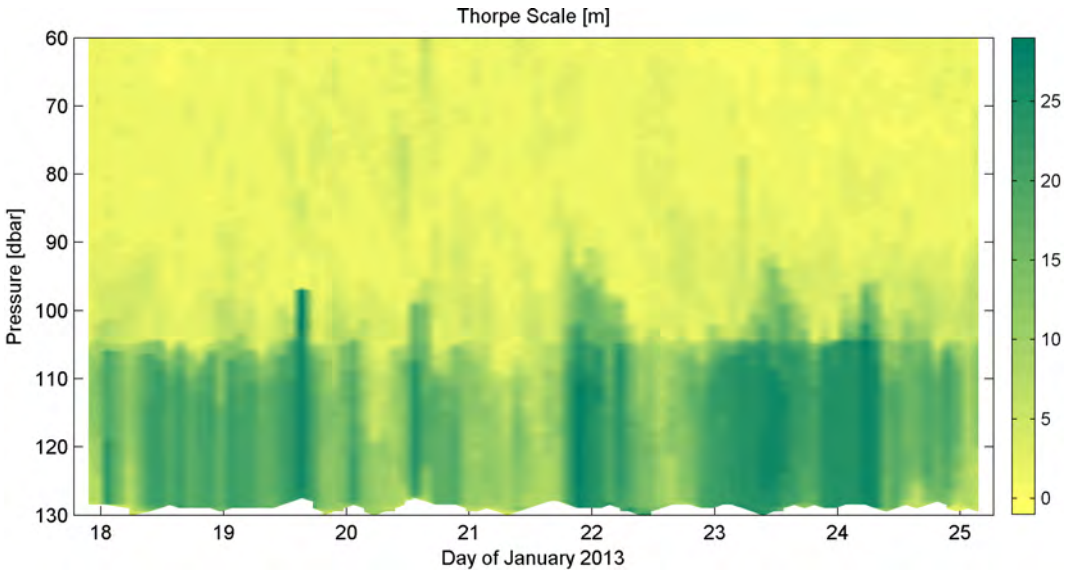

Figure 4.14: Time series of the Thorpe length scale L_T in the lower half of the water column on the inner shelf off Walvis Bay.

of about 2 m to a maximum of about 7 m above the bottom during that eight-day period.

The bottom shear stress τ_b derived from the estimated shear was on average 0.0090 Pa and at maximum 0.0310 Pa on the inner shelf off Walvis Bay. These results are in agreement with the findings of Monteiro et al. (2005). However, they stated that a critical bottom shear stress of 0.05 Pa is necessary to suspend sediments from the seafloor. This implies that during the eight-day period, the observed bottom shear stress on the mud belt was not even close to being strong enough to cause re-suspension.

In order to basically compare the variability of the measured ε in the near bottom layer (Section 4.6) with the variability of the estimated ε_s of the shear turbulence, both quantities have been depth averaged from 120 m to 127 m. The upper limit was chosen as a suitable depth level in agreement with the previous findings and the lower limit represents the deepest depth level at which a value for the measured ε exists for every time step. The resulting time series and the corresponding correlation coefficient r are shown in the bottom graph of Figure 4.16. It is immediately apparent that the measured ε and estimated ε_s adequately correspond with one another. The fluctuations of both quantities happen at similar pace, with similar intensities and at similar times. This visible assessment is supported by the high correlation coefficient of $r = 0.80$. The major differences between the two TKE dissipation rates mainly occur during periods of relatively small values of ε. Possible explanations may be the relatively high noise level of 10^{-9} W/kg of the free-falling microstructure probe as well as the impact of other dynamical processes, which generate small turbulent mixing in the near bottom layer.

The complete opposite is the case for the two previously described processes. The top graph of Figure 4.16 compares the variability of the power of the surface waves, which was obtained during the investigation of the swell in Section 4.4, with the variability of the depth averaged, measured ε in the near bottom layer. The middle graph of Figure 4.16 contrasts the variability of the temperature variance, which was received at the end of the investigations of the NLIW in Section 4.5, with the variability of the depth averaged, measured ε in the near bottom layer. By looking at both graphs, one can easily conclude that no correlation is present in both cases, respectively.

In summary, the study of different dynamical processes and their associated variability in the considered eight-day period in January 2013 revealed that the shear of the horizontal currents in the near bottom layer primarily determine the variability of the observed turbulence in the near bottom layer on the inner shelf off Walvis Bay. Moreover, swell and non-linear internal waves seem to have a negligible or minor impact on the variability of the turbulence in the near bottom layer on the inner shelf off Walvis Bay.

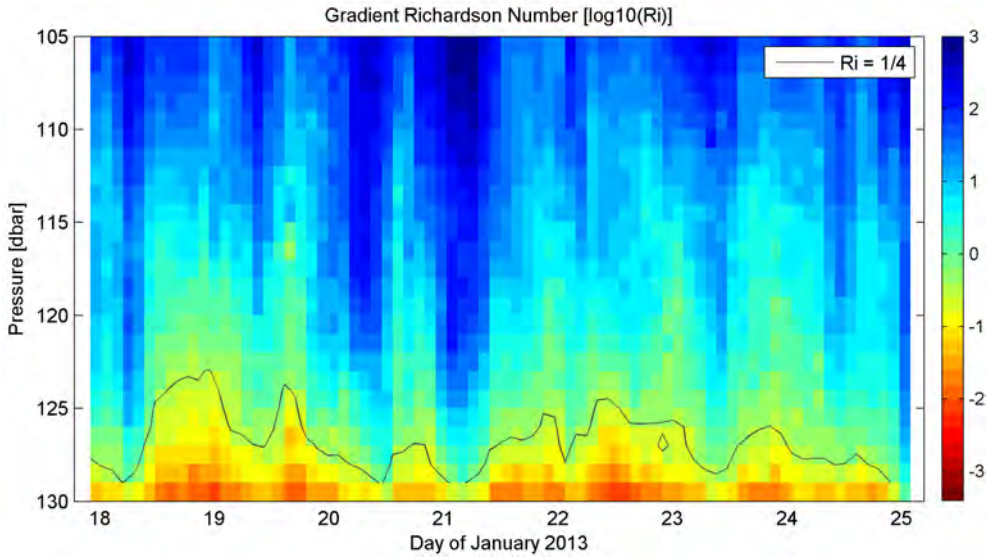

Figure 4.15: Time series of the gradient Richardson number (Ri) in the near bottom layer on the inner shelf off Walvis Bay. The contour plot is drawn for the logarithm of Ri. The black isoline represents the critical value $Ri = 0.25$.

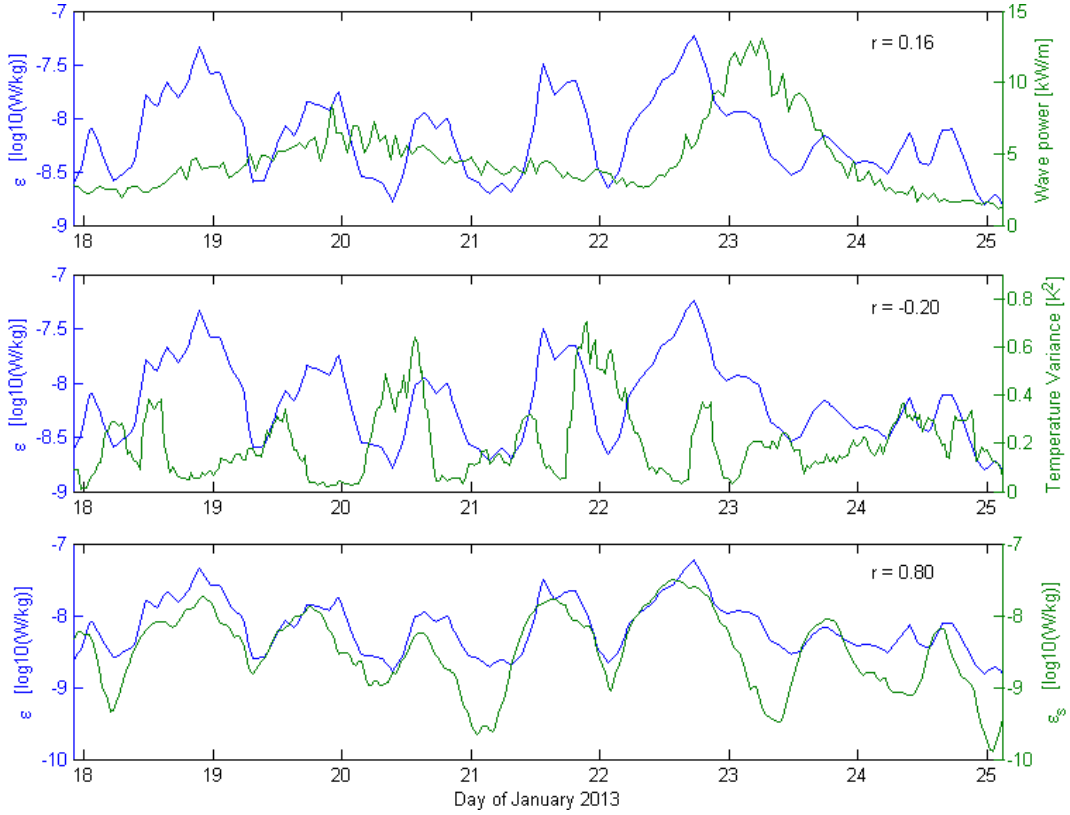

Figure 4.16: Comparison of the variability of the measured turbulence in the near bottom layer with the variability of the in detail discussed processes. At the top, the observed depth averaged (120 m to 127 m) TKE dissipation rate (blue curve) is shown together with the derived wave power of the swell investigations (green curve). In the middle, the observed depth averaged TKE dissipation rate (blue curve) is shown together with the derived temperature variance of the NLIW investigation (green curve). At the bottom, the observed depth averaged TKE dissipation rate (blue curve) is shown together the with the estimated TKE dissipation rate from the shear turbulence (green curve). The correlation coefficient between every two compared time series is given in the top right corner of every sub-figure.

4.7 Characteristics of turbulence across the central Namibian shelf

After the detailed investigation of the turbulent characteristics on the inner shelf off Walvis Bay, the essential features across the central Namibian shelf are now being examined.

Figure 4.17 illustrates the cross section of the TKE dissipation rate along the 23°S line across the central Namibian shelf. The underlying measurements across the Walvis Bay transect were performed from the 5 to 9 February 2011 during the RV Maria S. Merian cruise MSM17/3 (Mohrholz et al., 2011).

Across the entire shelf, the surface layer exhibits high dissipation rates, generated by wind mixing and ship induced disturbance. Below the thermocline, the dissipation rate in the open ocean was much weaker (10^{-9} W/kg), which is roughly the noise level of the microstructure profiler. In contrast, at the shelf breaks, the vertical displacement of isotherms indicates the instability of shoaling internal tides (Nash et al., 2004), which enhance the intensity of ε in the whole water column by an order of magnitude. In general, relatively high dissipation rates are observable when the bottom depicts a critical steepness, which is consistent with previous observations (see Subsection 2.2.2 for the details). In contrast, the smooth areas of the inner shelf show comparatively low dissipation rates. Having again in mind the described distribution of the mud belts across the shelf in mind (see Section 1.4), it is obvious that the locations with strong turbulence go along with the gaps between the mud belts. This supports the findings and hypothesis of Monteiro et al. (2005) and Inthorn et al. (2006b).

The described observations are emphasized by the illustrations in Figure 4.18. This figure compares the time-averaged vertical profile of ε on the shelf break in a water depth of around 400 m (Figure 4.18(a)) with the time-averaged vertical profile of ε on the inner shelf in a water depth of 130 m (Figure 4.18(b)). The underlying time series of the shelf break position was gathered at a 34 h station during the cruise DIS356 with the RRS Discovery from 7 October at 10 UTC to the 9 October at 8 UTC at the 23°S transect 75 nm off Walvis Bay (Mohrholz et al., 2010). The underlying time series on the inner shelf is the well-known eight-day period in January 2013 at 20 nm off Walvis Bay (see Figure 4.7).

The vertical profile of ε at the shelf break site reveals a surface mixed layer depth of around 50 m and a thickness of the turbulent bottom boundary layer in the range of 50 m to 100 m depth. Moreover, the values of ε in the interior of the water column fall only below $10^{-8.5}$ W/kg in the depth range from 200 m to 300 m depth (Figure 4.18(a)). If these findings are compared to the vertical profile of ε at the inner shelf location, significant differences are observable. The surface mixed layer reveals a depth of around 30 m and the turbulent bottom boundary layer extends to about 20 m above the seafloor. Between these two turbulent boundary layers, ε is always below the value of $10^{-8.5}$ W/kg.

These observations clearly highlight that the dynamic regimes are substantially different between the shelf break area with steep topography and the inner shelf location with a nearly horizontal seafloor.

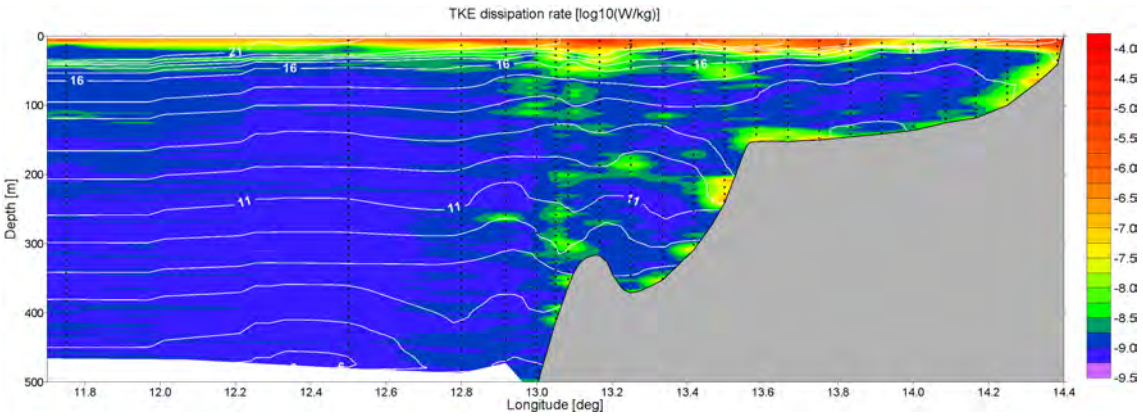

Figure 4.17: Patterns of the dissipation rate of the turbulent kinetic energy (contour plot) and temperature stratification (white isolines in [°C]) along the Walvis Bay transect. Taken from Mohrholz et al. (2011).

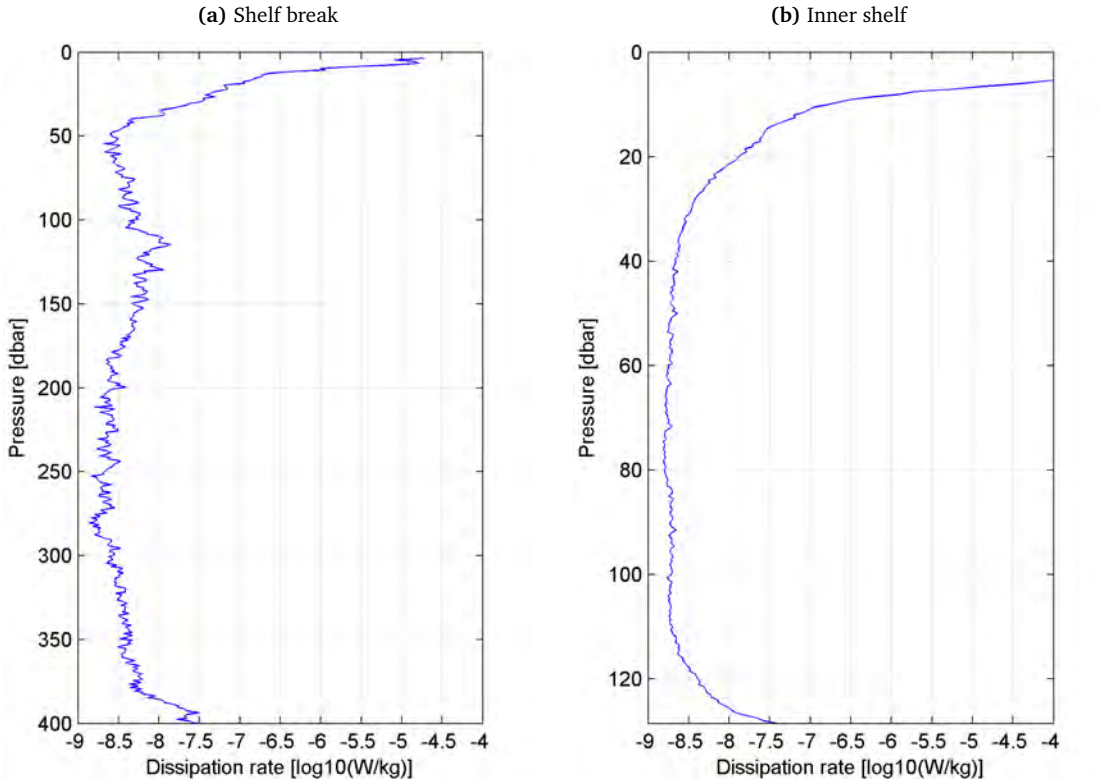

Figure 4.18: Comparison of time averaged TKE dissipation rates above the shelf break (a) at 75 nm off Walvis Bay and above the inner shelf (b) at 20 nm off Walvis Bay.

Chapter 5

Discussion and conclusion

The thesis attempts to improve the understanding of the short-term variability of the turbulent processes in the near bottom layer on the central Namibian shelf. A combination of field observations and remote sensing data was used to investigate the hydrographic conditions on the northern Namibian shelf from 18 to 25 January 2013.

Low wind speeds reduced the strength of the wind-driven coastal upwelling off Walvis Bay. Nevertheless, the cross shelf temperature and salinity transects at 23°S depict a thermohaline pattern, which is typical for upwelling regions. Furthermore, CTD measurements revealed very low oxygen concentrations in the bottom waters on the shelf that indicate hypoxic and anoxic conditions, which appear to result from a combination of local remineralisation of organic matter, as well as advection of remotely sourced oxygen poor water (e.g. Bartholomae and van der Plas, 2007).

The study of measured TKE dissipation rates in the lower half of the water column demonstrated increased turbulent mixing within the bottom boundary layer with a varying thickness of up to 25 metres. The intervals of enhanced TKE dissipation rates revealed a strong variability on various time scales, which suggest that a superposition of processes lead to the observed turbulence in the near bottom layer. The study about the reasons for the near bottom turbulence and its variability took over the main part of the investigations.

In search of the essential dynamic processes on the inner shelf off Walvis Bay, power spectral analyses of both a pressure and a current time series were performed. Significant peaks were observed at characteristic frequencies for swell, semidiurnal tidal oscillations, diurnal and inertial motions and low-frequency processes, such as CSW and CTW. Thereby, most of the energy is contained in the inertial and low-frequency motions. A supplementary harmonic analysis revealed that the significant tidal motions on the inner shelf off Walvis Bay are composed by the semidiurnal constituents M2, S2 and N2, whereby their corresponding current vector rotates on an elliptical path in an anticlockwise sense. These results are in good agreement with the conclusions of Lass and Mohrholz (2005).

Recent works (e.g. Herbers et al., 2000; Ardhuin et al., 2003) showed that swell can cause turbulent mixing in the near bottom layer on the shallow continental shelf of North Carolina. These findings motivated the detailed investigations of the swell on the central Namibian shelf in this thesis. Three moderate swell events were observed during the eight-day period in January 2013. The correlation of the time series of the surface wave power together with the time series of the TKE dissipation rate revealed that the occurrence of surface swell does obviously not contribute to turbulent mixing in the near bottom layer on the inner shelf off Walvis Bay. Apparently, the inner shelf seems to be too deep, so that surface gravity from the observed moderate swell events cannot produce measurable turbulence in the near bottom layer. Anyhow, since a swell-induced turbulent boundary layer extends only a few centimetres above the bottom (Grant and Madsen, 1986; Brink, 2004), it is certainly difficult to measure the impact with a microstructure profiler in 130 m depth. Improvements of the measurement setup could maybe open the possibility to find out, if, during periods of very energetic swell, sediments are being re-

suspended due to the wave motions on the inner shelf and then afterwards re-distributed by near bottom currents.

Furthermore, the occurrence and variability of NLIW on the inner shelf off Walvis Bay was studied to identify times when many intense and consecutive NLIW pass the mooring location. The observed variability depicts a slightly vague diurnal intermittency, which could indicate that they are generated by internal tides in the shelf break area (Monteiro et al., 2005). Further investigations revealed that the variability of turbulent mixing in the near bottom layer cannot be related to the occurrence of NLIW on the inner shelf. According to these findings, it can be assumed that the bathymetric slope of the inner shelf is too small, so that NLIW can actually interact with the topography to force strong bottom mixing. As a result, the NLIW seem to just pass the inner shelf region without producing any significant turbulent mixing while they afterwards break near the coast.

Nevertheless, a positive connection was found between the shear-induced turbulence in the near bottom layer and the measured TKE dissipation. The variability of the calculated TKE dissipation rate from the shear of an estimated logarithmic current profile in the near bottom layer sufficiently coincides with that of the measured dissipation rate. Consequently, the induced turbulence from the shear of the horizontal velocities in the benthic boundary layer determines the turbulent mixing in that layer in the eight-day period.

The variability of the near bottom TKE dissipation rate depicts apparent time scales in a range between roughly one to a few days. Due to the lack of velocity data in the near bottom layer, it is unattainable to adequately discover the source of these fluctuations. However, the broad frequency range and results of the power spectral analysis indicate that a superposition of diverse processes influences the currents in the near bottom layer, such as sub-inertial CSW and CTW, inertial motions, tidal currents as well as pressure gradient currents. For the sake of completeness, it should be noted that the formation of magnitude of a complex current vector is a non-linear transformation leading to artificial frequencies in the time series, which may result in misinterpretations of the observed frequencies.

Due to strong coastal upwelling, cold nutrient-rich deep waters are injected into the surface mixed layer in the northern Benguela, enabling intense primary production. As a result, sedimenting organic matter contribute to the un-oxidised mud on the seafloor (Bremner, 1983). On the central Namibian shelf, the sediment distribution depicts an accumulation of carbon-rich sediments in three belt-like patterns parallel to the isobaths (e.g. Inthorn et al., 2006b). The impact of various processes, which contribute to the overall pattern, is still subject of scientific debate. In recent years, the interactions of internal tides with the local shelf topography was suggested as a forcing factor governing the large-scale distribution of particulate organic matter on the central Namibian shelf (Monteiro et al., 2005). This thesis showed that spots of intense TKE dissipation in the bottom layer were found at the shelf break zones and at the coast. These findings suggest that the interaction of onshore propagation NLIW with topography forces strong bottom mixing in those areas, which support the re-suspension of particulate organic matter by enhanced bed stresses and thus, are non-depositional areas (Monteiro et al., 2005; Inthorn et al., 2006b). In contrast, in the shadow of the outer shelf break and between the inner shelf break and the coast, zones with little TKE dissipation were found in the interior as well as the bottom layer, which facilitates the accumulation of sinking organic matter and thus maintains the anoxic mud belts. This indicates that the inner shelf slope is sub-critical for internal waves, which prevents non-linear interactions between the waves and the topography (see Section 2.2.2).

In summary, this work improved the understanding of the short-term variability of the turbulent process in the near bottom boundary layer and thus, contributes to the overall understanding of the dynamical processes on the central Namibian shelf. It became apparent that various processes influence the dynamic characteristics on the central Namibian shelf; hence, variabilities occur on a broad range of time scales. Moreover, the results have shown that different processes dominate the turbulent mixing at different sites on the shelf. Among other things, one consequence is that low stress at the seabed on the inner shelf off Walvis Bay supports the accumulation of light organic sediments. Due to missing current

data, the sources for the variability of the current shear, which mainly induces the turbulent mixing in the near bottom layer, could not be identified precisely. Albeit, future ADCP measurements of the velocities close to the bottom and the following spectral analysis would definitely be a possibility to answer this open question. Perhaps it is worth considering integrating these measurements, when the LTMB mooring is redeployed the next time. For further improvements of understanding of the dynamic processes on the central Namibian shelf, it would also be valuable to generate multi-day high-resolution time series at one of the shelf break sites, to examine the dominating local processes in detail and to also investigate the generation process of NLIW. Additionally, it would be worthwhile to repeat these high-resolutions measurements, which formed the basis of this thesis, in austral winter. Thus, it would be possible to find out whether seasonal effects play a role for turbulent mixing in near bottom layer.

An alternative approach to enhance the understanding of the dynamic processes and their impacts would be the comparison of observations with corresponding data of realistically forced numerical model simulations. However, the given results of this thesis present a number of challenges in developing comprehensive numerical models. From the physical perspective, these models must be able to at least simulate the transfer of energy from tides into the internal wave field accurately, contain a detailed resolution of the shelf topography and of course include parameterizations for short-time mixing events as breaking of internal waves.

Acknowledgment

First and foremost I offer my deep gratitude to my supervisor Volker Mohrholz who has supported me throughout my thesis with his friendly assistance, inspiring guidance and immense knowledge whilst allowing me the leeway to work in my own way. I am using this opportunity to express my gratitude to everyone who supported me with insightful comments and hard questions throughout my Master's thesis. I would also like to thank the Leibniz Institute for Baltic Sea Research Warnemünde (IOW), which provided me with the facilities required for my thesis project.

Bibliography

Airy, G. B. (1845). Tides and Waves. *Encyclopedia Metropolitana*, 192:241–396.

Alford, M. H. (2001). Internal Swell Generation: The Spatial Distribution of Energy Flux from the Wind to Mixed Layer Near-Inertial Motions. *Journal of Physical Oceanography*, 31:2359–2368.

Alford, M. H. (2003). Redistribution of energy available for ocean mixing by long-range propagation of internal waves. *Nature*, 423(March):159–162.

Apel, J. R. (2002). Oceanic Internal Waves and Solitons. In *An Atlas of Oceanic Internal Solitary Waves*, number May 2002, pages 1–40. \protect \ T1 \ textbraceleftthttp://www.internalwaveatlas.com/Atlas2_index.html}.

Ardhuin, F., O'Reilly, W. C., Herbers, T. H. C., and Jessen, P. F. (2003). Swell Transformation across the Continental Shelf. Part I: Attenuation and Directional Broadening. *Journal of Physical Oceanography*, 33:1921–1939.

Bailey, G. and Chapman, P. (1991). Short-term variability during an anchor station study in the southern Benguela upwelling system: Chemical and physical oceanography. *Progress in Oceanography*, 28:9–37.

Bakun, A. (1993). The California Current, Benguela Current, and Southwestern Atlantic Shelf Ecosystems: A Comparative Approach to Identifying Factors Regulating Biomass Yields. In Sherman, K., Alexander, L. M., and Gold, D. B., editors, *Large Marine Ecosystems, Stress, Mitigation and Sustainability*, pages 199–221. American Association for the Advancement of Science.

Bakun, A. and Nelson, C. (1991). The seasonal cycle of wind-stress curl in subtropical eastern boundary current regions. *Journal of Physical Oceanography*, 21:1815–1834.

Bartholomae, C. and van der Plas, A. (2007). Towards the development of environmental indices for the Namibian shelf, with particular reference to fisheries management. *African Journal of Marine Science*, 29(1):25–35.

Boyer, D., Cole, J., and Bartholomae, C. (2000). Southwestern Africa: Northern Benguela Current Region. *Marine Pollution Bulletin*, 41(1-6):123–140.

Bremner, J. M. (1983). Biogenic Sediments on the South West African (Namibian) Continental Margin. In Thiede, J. and Suess, E., editors, *Coastal Upwelling. Its Sediment Record. Part B: Sedimentary Records of Ancient Coastal Upwelling*, pages 73–104. Plenum Press.

Brink, K. (2004). Coastal Physical Processes Overview. In Robinson, A. and Brink, K., editors, *The Sea. The Global Coastal Ocean. Multiscale Interdisciplinary Processes*, volume 13, pages 37–59. Harvard University Press, Cambridge.

Brink, K. H. (1991). Coastal-Trapped Waves and Wind-Driven Currents Over the Continental Shelf. *Annual Review of Fluid Mechanics*, 23(1):389–412.

Burchard, H. and Umlauf, L. (2013). Marine Turbulence (Lecture notes).

Carr, M. E. and Kearns, E. J. (2003). Production regimes in four Eastern Boundary Current systems. *Deep-Sea Research Part II: Topical Studies in Oceanography*, 50:3199–3221.

Colosi, J. A., Beardsley, R. C., Lynch, J. F., Gawarkiewicz, G., Chiu, C.-S., and Scotti, A. (2001). Observations of nonlinear internal waves on the outer New England continental shelf during the summer Shelfbreak Primer study. *Journal of Geophysical Research*, 106(C5):9587–9601.

Cushman-Roisin, B. and Beckers, J.-M. (2011). *Introduction to geophysical fluid dynamics: physical and numerical aspects*. Academic Press, 2nd edition.

D'Asaro, E. A. (1985). The Energy Flux from the Wind to Near-Inertial Motions in the Surface Mixed Layer. *Journal of Physical Oceanography*, 15:1043–1059.

Demaison, G. and Moore, G. (1980). Anoxic environments and oil source bed genesis. *Organic Geochemistry*, 2(1):9–31.

Emeis, K. C., Brüchert, V., Currie, B., Endler, R., Ferdelman, T., Kiessling, a., Leipe, T., Noli-Peard, K., Struck, U., and Vogt, T. (2004). Shallow gas in shelf sediments of the Namibian coastal upwelling ecosystem. *Continental Shelf Research*, 24:627–642.

Fennel, W. (1999). Theory of the Benguela Upwelling System. *Journal of Physical Oceanography*, 29:177–190.

Gargett, A. and Garner, T. (2008). Determining Thorpe Scales from Ship-Lowered CTD Density Profiles. *Journal of Atmospheric and Oceanic Technology*, 25(9):1657–1670.

Gill, A. (1984). On the behavior of internal waves in the wakes of storms. *Journal of Physical Oceanography1*, 14(7):1129–1151.

Gill, A. and Clarke, A. (1974). Wind-induced upwelling, coastal currents and sea-level changes. *Deep Sea Research and Oceanographic Abstracts*, 21(1973):325–345.

Gill, A. E. and Schumann, E. H. (1974). The Generation of Long Shelf Waves by the Wind. *Journal of Physical Oceanography*, 4:83–90.

Godin, G. (1972). The analysis of tides. *University of Toronto Press*.

Grant, W. and Madsen, O. (1986). The continental-shelf bottom boundary layer. *Annual Review of Fluid Mechanics*, 18:265–305.

Grant, W. D. and Madsen, O. S. (1979). Combined wave and current interaction with a rough bottom. *Journal of Geophysical Research*, 84(8):1797.

Hart, T. J. and Currie, R. I. (1960). The Benguela Current. *Discovery reports*, 31:123–298.

Herbers, T. H. C., Hendrickson, E. J., and O'Reilly, W. C. (2000). Propagation of swell across a wide continental shelf. *Journal of Geophysical Research*, 105(C8):19,729–19,737.

Holloway, P. E. (1983). Internal Tides on the Australian North-West Shelf: A Preliminary Investigation. *Journal of Physical Oceanography*, 13:1357–1370.

Holloway, P. E. (1987). Internal hydraulic jumps and solitons at a shelf break region on the Australian North West Shelf. *Journal of Geophysical Research*, 92(C5):5405–5416.

Howard, L. N. (1961). Note on a paper of John W. Miles. *Journal of Fluid Mechanics*, 10(4):509–512.

Howarth, M. and Pugh, D. (1983). Observations of Tides over the Continental Shelf of North-West Europe. In Johns, B., editor, *Physical Oceanography of Coasral and Shelf Seas*, volume 35, chapter 4, pages 135–188. Elsevier.

Hutchings, L., Verheye, H., Huggett, J. A., Demarcq, H., Cloete, R., Barlow, R. G., Louw, D., and da Silva, A. J. (2006). Variability of Plankton with Reference to Fish Variability in the Benguela Current Large Marine Ecosystem - An Overview. In Shannon, V., Hempel, G., Malanotte-Rizzoli, P., Moloney, C., and Woods, J., editors, *Benguela: Predicting a Large Marine Ecosystem*, pages 91–124. Elsevier, Amsterdam.

Huthnance, J. (1981). Waves and currents near the continental shelf edge. *Progress in Oceanography*, 10:193–226.

Huthnance, J. (1995). Circulation, exchange and water masses at the ocean margin: the role of physical processes at the shelf edge. *Progress in Oceanography*, 35(95):353–431.

Inthorn, M., Mohrholz, V., and Zabel, M. (2006a). Nepheloid layer distribution in the Benguela upwelling area offshore Namibia. *Deep Sea Research Part I: Oceanographic Research Papers*, 53(8):1423–1438.

Inthorn, M., Wagner, T., Scheeder, G., and Zabel, M. (2006b). Lateral transport controls distribution, quality, and burial of organic matter along continental slopes in high-productivity areas. *Geology*, 34(3):205.

Kamphuis, J. W. (2010). *Introduction to coastal engineering and management*, volume 30. Advanced Series on Ocean Engineering, 2nd edition.

Karimpour, A. (2014). Ocean Wave Analyzing Toolbox. www.arashkarimpour.com. Last checked on 14-02-2015.

Kitade, Y. and Matsuyama, M. (2000). Coastal-trapped waves with several-day period caused by Windalong the Southeast Coast of Honshu, Japan. *Journal of Oceanography*, 56(1983):727–744.

Klymak, J., Legg, S., Alford, M., Buijsman, M., Pinkel, R., and Nash, J. (2012). The Direct Breaking of Internal Waves at Steep Topography. *Oceanography*, 25(2):150–159.

Knight, P., Howarth, M., and Rippeth, T. (2002). Inertial currents in the northern North sea. *Journal of Sea Research*, 47(3-4):269–284.

Kolmogorov, A. (1941). The local structure of turbulence in incompressible viscous fluid for very large Reynolds numbers. *Doklady Akademii Nauk Sssr*, 30(1890):301–305.

Lamb, K. G. (2014). Internal Wave Breaking and Dissipation Mechanisms on the Continental Slope/Shelf. *Annual Review of Fluid Mechanics*, 46(1):231–254.

Lass, H. U. and Mohrholz, V. (2005). On the fluctuations and vertical structure of the shelf circulation off Walvis Bay, Namibia. *Continental Shelf Research*, 25(12-13):1473–1497.

Lerczak, J. a., Hendershott, M. C., and Winant, C. D. (2001). Observations and modeling of coastal internal waves driven by a diurnal sea breeze. *Journal of Geophysical Research*, 106(C9):19,715–19,729.

Liu, K.-K., Iseki, K., and Chao, S.-Y. (2000). Continental margin carbon fluxes. In Hanson, R. B., Ducklow, H. W., and Field, J. G., editors, *The Changing Ocean Carbon Cycle*, pages 189–239. Cambridge University Press.

Mater, B. D., Schaad, S. M., and Venayagamoorthy, S. K. (2013). Relevance of the thorpe length scale in stably stratified turbulence. *Physics of Fluids*, 25.

Miles, J. W. (1961). On the stability of heterogeneous shear flows. *Journal of Fluid Mechanics*, 10:496–508.

Miller, S. T. K., Keim, B. D., Talbot, R. W., and Mao, H. (2003). Sea breeze: Structure, forecasting, and impacts. *Reviews of Geophysics*, 41(3):1–31.

Mohrholz, V., Bartholomae, C. H., van der Plas, a. K., and Lass, H. U. (2008). The seasonal variability of the northern Benguela undercurrent and its relation to the oxygen budget on the shelf. *Continental Shelf Research*, 28(3):424–441.

Mohrholz, V., Eggert, A., Junker, T., Nausch, G., Ohde, T., and Schmidt, M. (2014). Cross shelf hydrographic and hydrochemical conditions and their short term variability at the northern Benguela during a normal upwelling season. *Journal of Marine Systems*, 140:92–110.

Mohrholz, V., Heene, T., Muller, A., and Hansen, A. (2011). Report and preliminary results of FS Maria S. Merian cruise MSM17/3, Walvis Bay - Dakar, 30.1.-7.3.2011.

Mohrholz, V., Oesterle, S., Heene, T., and Beier, S. (2013). Report and preliminary results of FS Mirabilis Cruise MOM1301, Walvis Bay - Walvis Bay, 15.01.-31.01.2013.

Mohrholz, V., Schmidt, M., Heene, T., Muller, A., and Wasmund, N. (2010). Hydrographic cruise report of RRS Discovery Cruise D-356, Walvis Bay - Cape Town, 10.9.-13.10.2010.

Monteiro, P., Nelson, G., van der Plas, A., Mabille, E., Bailey, G., and Klingelhoeffer, E. (2005). Internal tide - shelf topography interactions as a forcing factor governing the large-scale distribution and burial fluxes of particulate organic matter (POM) in the Benguela upwelling system. *Continental Shelf Research*, 25(15):1864–1876.

Monteiro, P. M. S., van der Plas, a., Mohrholz, V., Mabille, E., Pascall, a., and Joubert, W. (2006). Variability of natural hypoxia and methane in a coastal upwelling system: Oceanic physics or shelf biology? *Geophysical Research Letters*, 33(16):L16614.

Monteiro, P. M. S. and van der Plas, A. K. (2006). Low oxygen water (LOW) variability in the Benguela system: Key processes and forcing scales relevant to forecasting. In Shannon, V., Hempel, G., Malanotte-Rizzoli, P., Moloney, C., and Woods, J., editors, *Benguela: Predicting a Large Marine Ecosystem*, volume 14, pages 71–90. Elsevier, Amsterdam.

Moum, J. N., Farmer, D. M., Shroyer, E. L., Smyth, W. D., and Armi, L. (2007). Dissipative Losses in Nonlinear Internal Waves Propagating across the Continental Shelf. *Journal of Physical Oceanography*, 37(7):1989–1995.

Moum, J. N., Farmer, D. M., Smyth, W. D., Armi, L., and Vagle, S. (2003). Structure and Generation of Turbulence at Interfaces Strained by Internal Solitary Waves Propagating Shoreward over the Continental Shelf. *Journal of Physical Oceanography*, 33(20):2093–2112.

Munk, W. (1981). Internal waves and small-scale processes. In Warren, B. A. and Wunsch, C., editors, *Evolution of physical oceanography*, pages 264–291. MIT press.

Nash, J. D., Kunze, E., Toole, J. M., and Schmitt, R. W. (2004). Internal tide reflection and turbulent mixing on the continental slope. *Journal of Physical Oceanography*, 34:1117–1134.

Nasmyth, P. W. (1970). *Oceanic turbulence*. PhD thesis, The University of British Columbia.

Nelson, G. (1989). Poleward Motion in the Benguela Area. In Neshyba, S., Mooers, C., Smith, R., and Barber, R., editors, *Poleward flows along eastern ocean boundaries*, pages 110–130. Springer-Verlag, New York.

Nelson, G. and Hutchings, L. (1983). The Benguela upwelling area. *Progress in Oceanography*, 12(3):333–356.

Olbers, D., Willebrand, J., and Eden, C. (2012). *Ocean Dynamics*. Springer Science & Business Media.

Pawlowicz, R., Beardsley, B., and Lentz, S. (2002). Classical tidal harmonic analysis including error estimates in MATLAB using T_TIDE. *Computers & Geosciences*, 28(8):929–937.

Prandke, H. and Stips, A. (1998). Test measurements with an operational microstructure-turbulence profiler: Detection limit of dissipation rates. *Aquatic Sciences*, 60(3):191–209.

Rippeth, T. P., Simpson, J. H., Player, R. J., and Garcia, M. (2002). Current oscillations in the diurnal - inertial band on the Catalonian shelf in spring. *Continental Shelf Research*, 22(2):247–265.

Rogers, J. and Bremner, J. M. (1991). The Benguela Ecosystem. Part VII. Marine-Geological Aspects. In Barnes, M., editor, *Oceanography and marine biology: An Annual Review 29*, pages 1–85. UCL Press, London.

Sandstrom, H. and Elliott, J. A. (1984). Internal tide and solitons on the Scotian Shelf: A nutrient pump at work. *Journal of Geophysical Research*, 89(C4):6415–6426.

Schumann, E. H. and Brink, K. H. (1990). Coastal-Trapped Waves off the Coast of South Africa: Generation, Propagation and Current Structures. *Journal of Physical Oceanography*, 20(8):1206–1218.

Shannon, L. (1985). The Benguela ecosystem. 1. Evolution of the Benguela, physical features and processes. In Barnes, M., editor, *Oceanography and marine biology: An Annual Review*, volume 23, pages 105–182. University Press.

Shannon, L. and Nelson, G. (1996). The Benguela: Large Scale Features and Processes and System Variability. In Wefer, G., Berger, W. H., Siedler, G., and Webb, D. J., editors, *The South Atlantic: Present and Past Circulation.*, pages 163–210. Springer-Verlag, Berlin.

Shannon, L. V. and O'Toole, M. J. (2003). Sustainability of the Benguela: ex Africa semper aliquid novi. In Hempel, G. and Sherman, K., editors, *Large marine ecosystems of the world: trends in exploitation, protection and research*, pages 227–253. Elsevier, Amsterdam.

Shillington, F. A. (1998). The Benguela Upwelling System off Southwestern Africa. In Brink, K. and Robinson, A., editors, *The Sea gloabal coastal ocean: regional studies and syntheses*, pages 583–604. Wiley, New York.

Shillington, F. A., Reason, C. J. C., Duncombe Rae, C. M., Florenchie, P., and Penven, P. (2006). Large Scale Physical Variability of the Benguela Current Large Marine Ecosystem (BCLME). In Shannon, V., Hempel, G., Malanotte-Rizzoli, P., Moloney, C., and Woods, J., editors, *Benguela: Predicting a Large Marine Ecosystem*, volume 14, pages 49–70. Elsevier, Amsterdam.

Simpson, J. H. (1998). Tidal Processes in Shelf Seas. In Brink, K. and Robinson, A., editors, *The Sea. The Global Coastal Ocean. Processes and Methods*, volume 10, pages 113–150. John Wiley & Sons Ltd, New York.

Simpson, J. H., Hyder, P., Rippeth, T. P., and Lucas, I. M. (2002). Forced oscillations near the critical latitude for diurnal-inertial resonance. *Journal of Physical Oceanography*, 32:177–187.

Snodgrass, F., Groves, G., Hasselmann, K., Miller, G., Munk, W., and Powers, W. (1966). Propagation of ocean swell across the Pacific. *Philosophical Transactions of the Royal Society of London. Series A, Mathematical and Physical Sciences*, 259(1103):431–497.

Soulsby, R. (1983). The Bottom Boundary Layer of Shelf Seas. In Johns, B., editor, *Physical Oceanography of Coastal and Shelf Seas*, volume 35 of *Elsevier Oceanography Series*, chapter 5, pages 189–266. Elsevier.

St. Laurent, L. and Garrett, C. (2002). The Role of Internal Tides in Mixing the Deep Ocean. *Journal of Physical Oceanography*, 32:2882–2899.

Stramma, L. and England, M. (1999). On the water masses and mean circulation of the South Atlantic Ocean. *Journal of Geophysical Research*, 104(C9):20863.

Summerhayes, C. P. (1983). Sedimentation of organic matter in upwelling regimes. In Thiede, J. and Suess, E., editors, *Coastal Upwelling. Its Sediment Record. Part B: Sedimentary Records of Ancient Coastal Upwelling*, pages 29–72. Plenum Press, New York.

Thorpe, S. (2007). *An introduction to ocean turbulence*. Cambridge University Press.

Tucker, M. J. and Pitt, E. G. (2001). *Waves in Ocean Engineering*. Elsevier Science.

van der Plas, A., Monteiro, P., and Pascall, a. (2007). Cross-shelf biogeochemical characteristics of sediments in the central Benguela and their relationship to overlying water column hypoxia. *African Journal of Marine Science*, 29(January 2015):37–47.

Venayagamoorthy, S. and Fringer, O. (2012). Examining breaking internal waves on a shelf slope using numerical simulations. *Oceanography*, 25(2):132–139.

Venayagamoorthy, S. K. and Fringer, O. B. (2007). On the formation and propagation of nonlinear internal boluses across a shelf break. *Journal of Fluid Mechanics*, 577:137.

Wang, B. (2002). Kelvin waves. In Holton, J. R., Curry, J. A., and Pyle, J. A., editors, *Encyclopedia of Atmospheric Sciences*, pages 1062–1068. Elsevier Science.

Whiteman, C. and Bian, X. (1996). Solar semidiurnal tides in the troposphere: Detection by radar profilers. *Bulletin of the American Society*, 77:529–542.

Wilcock, W. (2014). Practical Aspects of Filtering (Lecture Notes). http://www.ocean.washington.edu/courses/ess522/lectures/10_filtering.pdf. Last checked on 14-02-2015.

Woodhead, P., Hamukuaya, H., O'Toole, M. J., and McEnroe, M. (1998). Effects of oxygen depletion in shelf waters on hake populations off central and northern Namibia. In Shannon, L. and O'Toole, M. J., editors, *International Symposium, Environmental Variability in The South East Atlantic*, page 10. NATMIRC, Namibia.

Zhang, X., DiMarco, S. F., Smith, D. C., Howard, M. K., Jochens, A. E., and Hetland, R. D. (2009). Near-Resonant Ocean Response to Sea Breeze on a Stratified Continental Shelf. *Journal of Physical Oceanography*, 39:2137–2155.

Eidesstattliche Erklärung

Hiermit versichere ich, Tom Lange, eidesstattlich durch eigenhändige Unterschrift, dass ich die Arbeit selbständig und ohne Benutzung anderer als der angegebenen Hilfsmittel angefertigt habe. Alle Stellen, die wörtlich oder sinngemäß aus Veröffentlichungen entnommen sind, habe ich als solche kenntlich gemacht.
Die eingereichte schriftliche Fassung der Arbeit entspricht der auf dem elektronischen Speichermedium.
Ich versichere weiter, dass diese Arbeit noch nicht als Abschlussarbeit an anderer Stelle vorgelegen hat.

.....	.....
Ort, Abgabedatum	Unterschrift